

GRANDMA Observations of ZTF/*Fink* Transients during Summer 2021

V. Aivazyan^{1,2}, M. Almualla³, S. Antier^{4,5,6}, A. Baransky⁷, K. Barynova⁸, S. Basa⁹, F. Bayard¹⁰, S. Beradze^{1,2}, D. Berezin¹¹, M. Blazek¹², D. Boutigny¹³, D. Boust^{14,15}, E. Broens^{16,17}, O. Burkhonov¹⁸, A. Cailleau¹⁹, N. Christensen⁴, D. Cejudo²⁰, A. Coleiro⁶, M. W. Coughlin²¹, D. Datashvili^{1,2}, T. Dietrich^{22,23}, F. Dolon²⁴, J.-G. Ducoin^{25,26}, P.-A. Duverne²⁵, G. Marchal-Duval²⁵, C. Galdies^{27,28}, L. Granier²⁹, V. Godunova¹¹, P. Gokuldass³⁰, H. B. Eggenstein³¹, M. Freeberg³², P. Hello²⁵, R. Inasaridze^{1,2}, E. E. O. Ishida³³, P. Jaquiere³⁴, D. A. Kann¹², G. Kapanadze^{1,2}, S. Karpov³⁵, R. W. Kiendrebeogo^{4,36}, A. Klotz^{37,38}, R. Kneip³⁹, N. Kochiashvili¹, W. Kou⁴⁰, F. Kugel¹⁴, C. Lachaud⁶, S. Leonini⁴¹, A. Leroy^{42,43}, N. Leroy²⁵, A. Le Van Su²⁴, D. Marchais⁴⁴, M. Mašek³⁵, T. Midavaine⁶, A. Möller^{33,45}, D. Morris³⁰, R. Natsvlishvili¹, F. Navarete⁴⁶, K. Noysena⁴⁷, S. Nissanke⁵, K. Noonan⁴⁸, N. B. Orange⁴⁸, J. Peloton²⁵, A. Popowicz⁴⁹, T. Pradier⁵⁰, M. Prouza³⁵, G. Raaijmakers⁵, Y. Rajabov¹⁸, M. Richmond⁵¹, Ya. Romanyuk⁵², L. Rousselot⁵³, T. Sadibekova^{18,53}, M. Serrau¹⁴, O. Sokoliuk^{7,52}, X. Song⁴⁰, A. Simon^{55,56}, C. Stachie⁴, A. Taylor^{57,58,59}, Y. Tillayev^{18,60}, D. Turpin^{54*}, M. Vardosanidze^{1,2}, J. Vlieghe²⁵, I. Tosta e Melo⁶¹, X. F. Wang^{62,40}, J. Zhu⁴⁰

Accepted XXX. Received YYY; in original form ZZZ

ABSTRACT

We present our follow-up observations with GRANDMA of transient sources revealed by the Zwicky Transient Facility (ZTF). Over a period of six months, from 1 April to 30 September 2021, all ZTF triggers were examined in real time by a dedicated science module implemented in the *Fink* broker, which will be used for the data processing of the Vera C. Rubin Observatory. In this article, we present three selection methods to identify promising kilonova candidates. Out of more than 35 million candidates, a hundred sources have passed our selection criteria. Six were then followed-up by GRANDMA (by both professional and amateur astronomers). The majority were finally classified either as asteroids or as supernovae events. We then demonstrate the added value of a substantial follow-up campaign of optical transients. We mobilized 37 telescopes, bringing together a large sample of images, taken under various conditions and quality. To complement the orphan kilonova candidates (those without associated gamma-ray bursts, which were all), we included three additional supernovae alerts to conduct further observations of during summer 2021. We demonstrate the importance of the amateur astronomer community that contributed from one to 23 images within the first two days after the *Fink* alert for scientific analyzes of new sources discovered in a magnitude range $r' = 17 - 19$ mag. We based our rapid kilonova classification on the decay rate of the optical source that should exceed 0.3 mag/day. GRANDMA's follow-up determined the fading rate within 1.5 ± 1.2 days post-discovery, without waiting for further observations from ZTF. No confirmed kilonovae were discovered during our observing campaign. This work will be continued in the coming months in the view of preparing for kilonova searches in the next gravitational-wave observing run O4 and the commissioning of the Vera C. Rubin Observatory.

Key words: methods: observational – Stars: neutron – Gravitational waves:

1 INTRODUCTION

The landmark detection of GW170817 by LIGO and Virgo (Abbott et al. 2017a), GRB 170817A by Fermi-GBM (Goldstein et al. 2017) and INTEGRAL (Savchenko et al. 2017), and the subsequent accompanying host of electromagnetic signatures (Abbott et al. 2017b) solidified the long predicted connection of binary neutron star mergers (BNS) to short gamma-ray bursts (sGRBs; e.g., Alexander et al. 2017; Haggard et al. 2017; Hallinan et al. 2017), and optical/infrared transients called kilonovae (KNe; e.g., Andreoni et al. 2017; Arcavi et al. 2017; Hu et al. 2017). Signatures of KNe also exist in some sGRBs (e.g., Tanvir et al. 2013; Berger et al. 2013), and efforts to obtain a full characterization of their emission remain a major priority in Astrophysics. In particular, KN emission is uniquely suited to better constrain the neutron star equation of state (EoS, e.g., Bauswein et al. 2017; Margalit & Metzger 2017; Coughlin et al. 2018; Coughlin et al. 2019; Coughlin et al. 2020c), the Hubble constant (e.g., Abbott et al. 2017a; Hotokezaka et al. 2019; Dietrich et al. 2020; Coughlin et al. 2020a; Coughlin et al. 2020b) and the abundancies of r -process nucleosynthesis (e.g., Chornock et al. 2017; Coulter et al. 2017; Cowperthwaite et al. 2017).

To address outstanding questions related to KNe, e.g., answering whether or not diverse processes take place in their ejecta and the sources of different emission components, a large sample of sources are necessary (Andreoni et al. 2021a,b). However, obtaining such a large data set is a difficult task for several reasons. Firstly, KNe are rare ($< 1\%$ of the core collapse supernova rate), fast (rapidly fading $\gtrsim 0.5$ mag per day in the optical), and faint transients ($M \gtrsim -16$ at peak), e.g., see Andreoni et al. (2021a). Secondly, the typical protocol for identifying and studying KNe remains, for the most part, rapid follow-up of gravitational-wave (GW) and high-energy gamma-ray burst (GRB) triggers (e.g., Andreoni et al. 2021a,b). So far, only the BNS merger GW170817 has revealed a KN counterpart, and even with near-term improvements to GW monitoring networks only a few tens of triggers are anticipated throughout the upcoming decade (see Andreoni et al. 2019).

Current and future wide-field optical and near-infrared surveys have been recently employed as tools for discovering KNe (Andreoni et al. 2019, 2021a,b). The fundamental idea is to capitalize on real-time survey data for serendipitous transient discovery, as opposed to “triggered” observations that use timing and/or localization information from other wavelengths or messengers (Andreoni et al. 2021b). Active facilities applicable for serendipitous fast-transient discovery include the Panoramic Survey Telescope and Rapid Response System (Pan-STARRS; Morgan et al. 2012), Asteroid Terrestrial-impact Last Alert System (ATLAS; Tonry et al. 2018), the Dark Energy Camera (DECam; Flaugher et al. 2015), the Zwicky Transient Facility (ZTF; Bellm et al. 2019; Graham et al. 2019; Masci et al. 2019; Dekany et al. 2020; Ho et al. 2022) and the Gravitational-Wave Optical Transient Observer (GOTO; Gompertz et al. 2020), while future instrumentation include BlackGEM (Bloemen et al. 2015) and the Vera C. Rubin Observatory’s Legacy Survey of Space and Time (LSST; Ivezić et al. 2019).

The ZTF has been a particular focal point for serendipitous KN discoveries as its volumetric survey speed is sensitive to objects that are faint and fast-fading out to almost

200 Mpc (Andreoni et al. 2021b), and its alert stream design follows closely that envisioned for the LSST (Patterson et al. 2019). The ZTF was built upon the existing Palomar 48” telescope after being equipped with a custom-built wide-field camera (e.g., Bellm et al. 2019), and its observing system scans large areas of the sky several times each night in multiple bands ($g'r'i'$), with optical transients identified in near-real time using reference image subtraction (Dekany et al. 2020).

A first initiative (Andreoni et al. 2021b) was developed as the ZTF REaltime Search and Triggering (ZTFReST) to identify KNe in ZTF data, and autonomously rank candidates in the ZTF alert stream based on their photometric evolution and fitting to KN models. Though ZTFReST proved to be effective at serendipitously discovering extragalactic fast transients in the initial system-test trials carried out by Andreoni et al. (2021b), no KNe were identified. Such results, in addition to outcomes from simulation studies of Vera C. Rubin Observatory observations (e.g., Andreoni et al. 2021a), have raised the necessity of exploring alternate strategies for synoptic survey techniques and alert characterizations that are optimized to study the transient universe (e.g., see Andreoni et al. 2019; Almualla et al. 2020).

In this article, we propose a method to explore the detection and early characterization of potential KN candidates from the public data released by ZTF in real time. We use FINK¹ (Möller et al. 2020), a community broker for the upcoming LSST, which currently analyzes the public alert stream from the ZTF survey. We have built three specific selection algorithms (known as “filters”) to select the most promising KN candidates from the global alert streams. The KN filters are based on temporal light curve and color evolution, and will be explained in detail in Section 3.2.

We demonstrate the ability of the GRANDMA (Antier et al. 2020a,b) world-wide network of telescopes to respond quickly to ZTF-Fink alerts and provide complementary observations to ZTF data at very early times. From the actual cadence of ZTF, we expect a collection of consecutive points, taken with the same filter, to have ~ 2.5 days latency. However, works such as Coughlin et al. (2020d); Almualla et al. (2021) demonstrate that there is added value in obtaining a more refined sampling resolution for the light curve of the transient due to the fast-fading nature of KNe. Early-time observations are especially important in bluer bands such a B or g' , in which the KN is expected to fade even more quickly – becoming undetectable within on the order of one or two days. In addition, incorporating different filter combinations can help in distinguishing KNe from other candidate transients through their expected color evolution (Margutti et al. 2018; Cowperthwaite et al. 2019; Coughlin et al. 2020d).

The main challenge is not only to coordinate responses to alerts within 48 hours globally, but also to build a real-time data reduction pipeline that is able to digest heterogeneous data from a diverse set of telescopes in order to produce refined data in between consecutive ZTF observations. Although this general problem of calibration, explored for example in Perley et al. (2019); Brennan & Fraser (2022), is not new, it is crucial for the progress of transient and GW

¹ <https://fink-broker.org>

science. The larger objective is therefore to efficiently characterize all of the candidate transients through the use of optimal filter choices and multiple early-time observations, in order to rapidly rule out (or confirm) the nature of the transient as a KN.

We organized an observational campaign from 21 May 2021 to 21 September 2021, named “ReadyforO4” (RO4), to invite members of GRANDMA (both professional and amateur astronomers) to follow-up KN candidates from ZTF-Fink in order to enable the early characterization of the detected transients. The paper is organized as follows: Section 2 introduces the GRANDMA consortium, and its citizen science program, Kilonova-catcher. Section 3 provides details on the KN filters used in this work, provided by FINK in collaboration with GRANDMA. Section 4 presents the GRANDMA observations of the RO4 campaign, general data reduction, accuracy of real-time scoring and the results for non-confirmation of KNe. We finish by presenting our conclusions in Section 5.

2 GRANDMA AND KILONOVA CATCHER

The GRANDMA (Global Advanced Rapid Network Devoted to Multi-messenger Addicts) consortium is a world-wide network of 30 telescopes from 23 observatories, 42 institutions, and groups from 18 countries (e.g., see Antier et al. 2020a,b). These facilities make available large amounts of observing time that can be allocated for photometric and/or spectroscopic follow-up of transients. The network has access to wide field-of-view telescopes ([FoV] $> 1 \text{ deg}^2$) located on three continents, and remote and robotic telescopes with narrower fields-of-view as reported in Table 1.

New telescopes have joined the network since the third LIGO-Virgo observational run O3 (which was described in Antier et al. 2020a,b). In particular, the collaboration with Thailand has provided an opportunity to access both the Southern and Northern sky by Thai Robotic Telescopes (TRTs) located at Springbrook Observatory (TRT-SBO) in Australia and Sierra Remote Observatory (TRT-SRO) in USA.

The 50cm Ali telescope of the Beijing Planetarium, Beijing Academy of Science and Technology, performs both astronomy research and public outreach functions. It is located in the Ngari region of Tibet. It is a 20'' reflecting telescope equipped with a 22.5mm \times 22.5mm CMOS camera. The 5 σ magnitude limits are expected to be $g' > 20 \text{ mag}$ in single images.

A 38cm Schmidt-Cassegrain (with f/11 equipped with a ST-8 CCD sensor) was used at the Lisnyky Observatory granted by the Main Astronomical Observatory of National Academy of Sciences of Ukraine.

The ICAMER Observatory of NAS of Ukraine provided observations with the 60cm Zeiss at the Terskol Observatory located in the North Caucasus.

In addition, the 1m telescope in Pic du Midi is being renovated by the IRAP laboratory and will participate in the GRANDMA consortium, as well as the 1.6m Perkin-Elmer telescope located at Pico dos Dias Observatory in Brazil. All characteristics of the new partners can be found in Table 1.

Within 24 hours, the GRANDMA network is able to access more than $\sim 72\%$ of the sky (up to more than 80%)

to a limiting magnitude of $\sim 18 \text{ mag AB}$. Due to a less dense distribution of Western Hemisphere observatories, the sky coverage is reduced to 49 – 60% during the night in the Americas. GRANDMA has access to four spectroscopic instruments with sensitivity down to $\approx 22 \text{ mag}$ as shown in Table 2. In particular, the High-Energy Transients and their Hosts (HETH) group at the Instituto de Astrofísica de Andalucía has access to two telescopes via competitive proposals for orphan KNe. At the Centro Astronómico Hispano en Andalucía (CAHA), Almeria, Spain, we obtained observing time (PI: Kann) at the 2.2m telescope (equipped with the CAFOS and BUSCA optical imagers) and the 3.5m telescope (with the $\Omega 2000$ infrared imager). Two nights of $\Omega 2000$ time were granted. At the 10.4m Gran Telescopio Canarias (GTC), we obtained observing time (PI: Kann) with three instruments: the optical imager and spectrograph OSIRIS (8 hrs), the infrared imager and spectrograph EMIR (5 hrs), and finally the integral-field-unit spectrograph MEGARA (2 hrs) to obtain late-time 3D spectroscopy of KN host galaxies. As this is competitive time, we were more conservative with triggering; in particular the GTC proposal was focused on obtaining data from confirmed KNe only. Therefore no observations were obtained during this campaign. Finally, GRANDMA obtained 6 h time allocated by CFHT/WIRCAM (using NIR JHK_S filters) in 2021A and 2021B that were not used due to the lack of confirmed KNe.

In 2019, GRANDMA initiated the creation of an innovative citizen science program called *Kilonova-Catcher*, hereafter KNC (Antier et al. 2020a). It aims at incorporating amateur astronomers into the search for and follow-up of fast transients such as GRBs and KNe. The GRANDMA consortium has already demonstrated its ability to forward the alerts of the O3 observing run to the amateur astronomers and to provide customized observation plans to each KNC astronomer; in return, they transfer images to the GRANDMA server to be analyzed afterwards. This process creates a continuous chain of observations at very early times after the alerts, before passing the responsibilities to the larger-aperture telescopes of the professional community. KNC uses a dedicated portal² to organize its activities, while the GRANDMA consortium is in charge of the data analysis of the images (see Section 4). In Fig. 1, we show the locations of the KNC telescope network.

3 METHOD: SEARCHING FOR KILONOVAE USING THE FINK BROKER

3.1 FINK overview

FINK (Möller et al. 2020) is a community broker designed to enable science with large time-domain alert streams such as the one from the current ZTF survey or the upcoming LSST. Driven by its scientific community, FINK probes a large number of topics in the transient sky, from solar system science to galactic, and extra-galactic science.

FINK currently analyzes the public alert data stream

² <http://kilonovacatcher.in2p3.fr/> supported by the University of Paris and the IJCLab institute

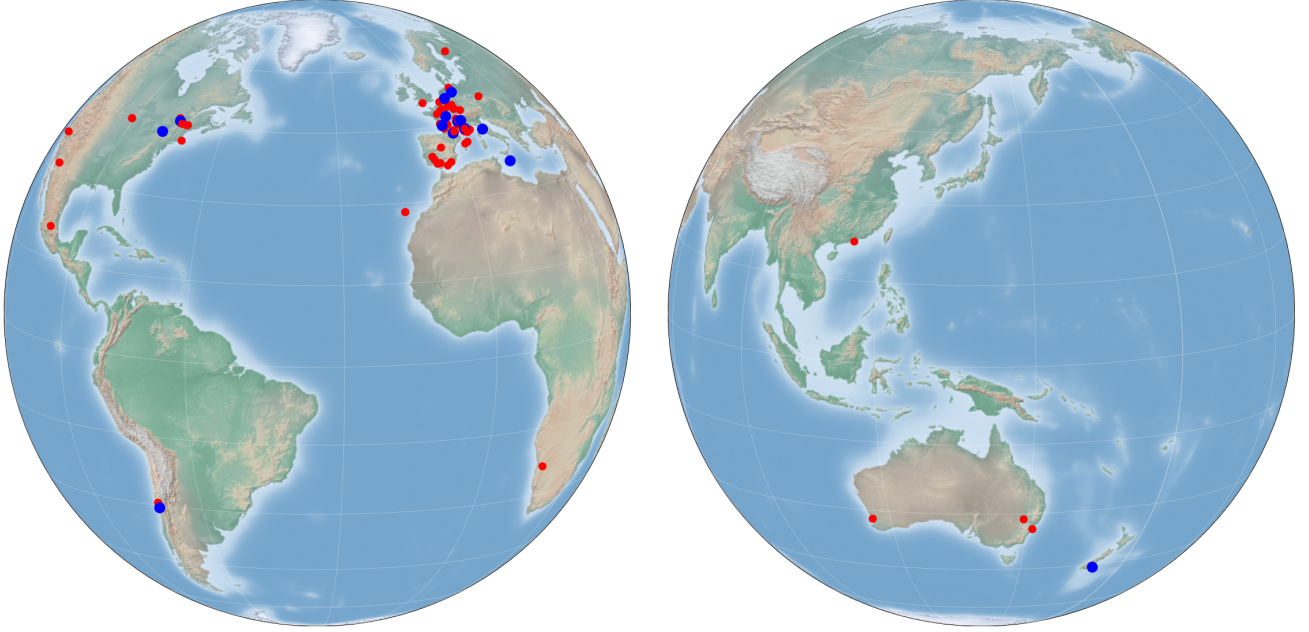


Figure 1. Locations of the 77 telescopes involved in the GRANDMA citizen science program *Kilonova-Catcher*. In blue are the telescopes used in this study, in red, the rest of the network.

Table 1. List of telescopes of the GRANDMA consortium and their photometric performance when using their standard setup. In blue are mentioned the ones that were engaged in observations for this work.

Telescope Name	Location	Aperture (m)	FOV (deg)	Filters	3σ limit (AB mag)	Max. Night slot (UTC)
TRT-SBO	Sierra Remote Obs.	0.70	0.17×0.17	$UBVR_CI_C$	19.0 in 60s (Clear)	00h-10h
TAROT/TCH	La Silla Obs.	0.25	1.85×1.85	Clear, $g'r'i'$	18.0 in 60s (Clear)	00h-10h
TRT-SRO	Springbrook Research Obs.	0.70	0.17×0.17	$UBVR_CI_C$	19.0 in 60s (Clear)	10h-16h
CFHT/WIRCAM	CFH Obs.	3.6	0.35×0.35	JHK_S	22.0 in 200s (J)	10h-16h
FRAM-Auger	Pierre Auger Obs.	0.30	1.0×1.0	BVR_CI_C , Clear	17.0 in 120s (R_C)	00h-10h
CFHT/MEGACAM	CFH Obs.	3.6	1.0×1.0	$g'r'i'z'$	23.0 in 200s (r')	10h-16h
Thai National Tel.	Thai National Obs.	2.40	0.13×0.13	Clear, $u'g'r'i'z'$	22.3 in 3s (g')	11h-23h
Zadko	Gingin Obs.	1.00	0.17×0.12	Clear, $g'r'i'IC$	20.5 in 40s (Clear)	12h-22h
TNT	Xinglong Obs.	0.80	0.19×0.19	$BVg'r'i'$	19.0 in 300s (R_C)	12h-22h
Xinglong-2.16	Xinglong Obs.	2.16	0.15×0.15	$BVRI$	21.0 in 100s (R_C)	12h-22h
GMG-2.4	Lijiang Obs.	2.4	0.17×0.17	$BVRI$	22.0 in 100s (R_C)	12h-22h
BJP/ALI-50	Ali Obs.	0.5	0.38×0.38	Clear, $g'r'$	20.8 in 20s (Clear)	14h-00h
UBAI/NT-60	Maidanak Obs.	0.60	0.21×0.21	BVR_CI_C	18.0 in 180s (R_C)	14h-00h
UBAI/ST-60	Maidanak Obs.	0.60	0.23×0.23	BVR_CI_C	18.0 in 180s (R_C)	14h-00h
TAROT/TRE	La Reunion	0.18	4.2×4.2	Clear	16.0 in 60s (Clear)	15h-01h
Les Makes/T60	La Reunion.	0.60	0.3×0.3	Clear	19.0 in 180s (Clear)	15h-01h
Terskol/Zeiss-600	Terskol Obs	0.6	0.18×0.18	Clear, BVR_CI_C	21.5 in 120s (R_C)	16h-02h
Abastumani/T70	Abastumani Obs.	0.70	0.5×0.5	BVR_CI_C	18.2 in 60s (R_C)	17h-03h
ShAO/T60	Shamakhy Obs.	0.60	0.28×0.28	BVR_CI_C	19.0 in 300s (R_C)	17h-03h
Lisnyky/AZT-8	Kyiv Obs.	0.70	0.38×0.38	$UBVR_CI_C$	20.0 in 300s (R_C)	17h-03h
Lisnyky/Schmidt	Kyiv Obs.	0.36	0.20×0.14	Clear, $UBVR_CI_C$	19.5 in 300s (R_C)	17h-03h
TAROT/TCA	Calern Obs.	0.25	1.85×1.85	Clear, $g'r'i'$	18.0 in 60s (Clear)	20h-06h
FRAM-CTA	ORM	0.25	0.43×0.43	Clear, BVR_Cz' ,	16.5 in 120s (R_C)	20h-06h
IRIS	OHP	0.50	0.4×0.4	Clear, $u'g'r'i'z'$	18.5 in 60s (r')	20h-06h
T120	OHP	1.20	0.3×0.3	BVR_CI_C	20.0 in 60s (R)	20h-06h
Pic du Midi/T1M	Pic du Midi	1.05	0.13×0.13	$u'g'r'i'z'$	19.5 in 60s (r')	20h-06h
2.2m CAHA/CAFOS	Calar Alto Obs.	2.20	0.27 (D)	$u'g'r'i'z'$	23.7 in 100s (r')	20h-06h
3.5m CAHA/ Ω 2000	Calar Alto Obs.	3.50	0.257×0.257	JHK_S	20 in 90s (J)	20h-06h
10.4m GTC/OSIRIS	ORM.	10.40	0.13×0.13	$u'g'r'i'z'$	24 in 30s (r')	20h-06h
10.4m GTC/EMIR	ORM.	10.40	0.111×0.111	$YJHK_S$	24 in 120s (Y)	20h-06h
VIRT	Etelman Obs.	0.50	0.27×0.27	$UBVR_CI_C$, Clear	19.0 in 120s (Clear)	22h-04h
Perkin-Elmer Tel.	Pico dos Dias Obs	1.6	0.083×0.083	$UBVR_CI_C$	21 in 360s (Clear)	18h-01h

Table 2. List of telescopes of the GRANDMA consortium with spectroscopic capabilities.

Telescope/Instrument	Location	Wavelength range	Spectral resolution $\lambda/\Delta\lambda$	Limiting mag
2.2m CAHA/CAFOS	Calar Alto Obs.	3200-7000/6300-11000	400	20 in 1h
ShAO/T2m	Shamakhy Obs.	3800 – 8000	2000	17 in 1h
Terskol-2m/MMCS	Terskol Obs.	3800 – 9000	1200	17 in 1h
Xinglong-2.16/BFOSC	Xinglong Obs.	3600 – 9600	1000	18 in 1h
GMG-2.4/YFOSC	Lijiang Obs.	3400 – 9100	2000	19 in 1h
10.4m GTC/OSIRIS	ORM	3630 – 7500/7330 – 10000	1018/2503	24 in 1h
10.4m GTC/EMIR	ORM	890 – 13310	987	21 in 1h

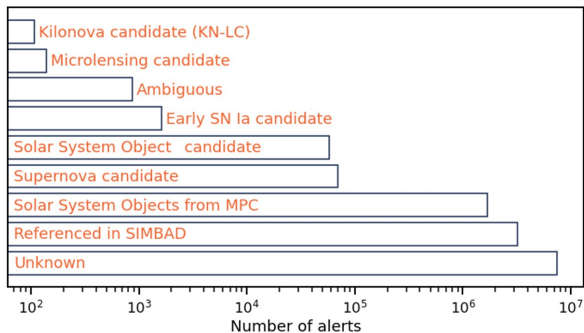


Figure 2. FINK classification labels for the 12,556,539 ZTF alerts that passed the quality cuts in the period 01 April to 30 September, 2021. About half of the alerts got no classification (Unknown label), i.e., FINK was not able to conclude on the nature of the alert given the alert information available. The remaining half is dominated by objects with a counterpart in the SIMBAD database (match within $1''.5$ radius), and alerts associated with a known object from the Minor Planet Center database (moving objects from the Solar System). Other alerts are associated with supernova events, Solar System Object candidates, microlensing candidate events, or have an ambiguous classification (more than one label at a time). Concerning KN candidates, we report here the 107 alert candidates from the KN-LC filter (see text below).

from the ZTF survey. Each night, alerts are collected in real-time after their processing by ZTF. FINK received 35,387,098 alerts between 01 April and 30 September 2021 (160 observing nights). Alerts carry out basic measurements for the trigger (position, magnitude, time), but also the detections that occurred up to 30 days before the alerts at the same location in the sky, allowing to reconstruct at least a partial light curve of the potential candidate. All incoming alerts are stored on disk, but only alerts with sufficient quality are then processed. At the time of the campaign, there were three quality cuts in FINK to assess the quality of alerts and reject artefacts and known bogus alerts (Möller et al. 2020); these cuts discarded about 70% of the incoming alerts.

The remaining 30% of alerts (12,556,539 alerts) are then processed by the FINK science modules. Science modules are provided by the community of users to add value to alerts, as detailed below. We note that the state of the broker constantly evolves over time (additions, or corrections), and we report results using `fink-broker` version 1.1, `fink-science` version 0.4, and `fink-filters` version 0.2. There are several types of added values: labels from the cross-match with external catalogs or survey feeds, classification scores provided by a machine learning analysis, or simply tags based on the alert content. These added values are then combined

to provide a unique classification for each alert. Fig. 2 shows the alert classification during the KNC observational campaign. About half of the alerts got classified, i.e., FINK can extract information about the potential nature of the object. Most of the classified alerts are cataloged in the SIMBAD database³. For the KN classification, we describe and report below the candidates from the KN-LC filter.

3.2 Kilonova candidate selection

Our main goal is to identify the most probable KN candidates among all incoming alerts. There are two competing factors: criteria that are too broad would yield too many candidates to follow up, given the huge number of incoming alerts; on the other hand, complex selection criteria would be meaningless given the lack of actual KN observations to constrain the parameter space.

In order to optimize our search for KNe, we designed three selection filters targeting different likely aspects of a KN. They act at the end of the FINK processing to reduce the incoming data stream and to select the most probable KN candidates. In the period of 01 April to 30 September 2021 we obtained:

- Machine learning-based filter (KN-LC): 107 alert candidates
- Near-by Galaxy Catalogs-based filter (KN-Mangrove): 68 alert candidates
- Rate-based filter (KN-Slope): 127 alert candidates

We note that only five alert candidates were selected by more than one filter, showing that the filters are triggered by different parameters of the incoming alerts. Hence, alerts selected by more than one filter are particularly noteworthy. All filters are open-source and can be found at <https://github.com/astrolabsoftware/fink-filters>. A detailed description and analysis of the filter outputs can be found in the accompanying notebook⁴.

3.2.1 Machine learning-based filter (KN-LC)

This filter mainly uses information from the light curve. During the classification step, the FINK classifier extracts features from the light curves in the g' and r' photometric bands (see Biswas et al., in prep.) and infer the probability of an alert being a KN. The light curves are deconstructed as a linear combination of principal components, and additional features are also extracted such as the maximum of the

³ <https://www.minorplanetcenter.net/>

⁴ https://github.com/astrolabsoftware/fink_grandma_kn

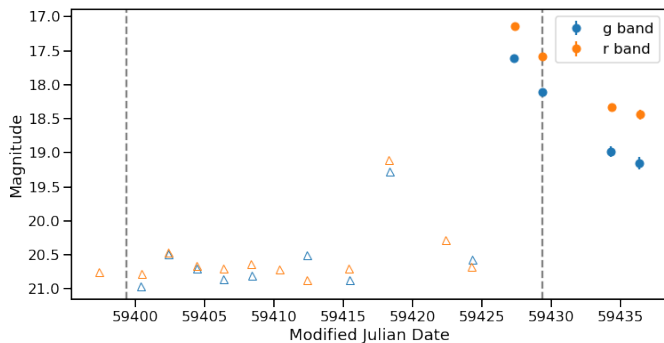


Figure 3. ZTF object light curve of one kilonova candidate from the KN-LC filter. Circles with error bars show valid alerts (detections) that pass the FINK quality cuts. Downward-pointing open triangles represent 5σ magnitude limits in template-subtracted difference images based on point-spread-function (PSF) fit photometry contained in the history of valid alerts. The right-most vertical line shows the KN trigger by FINK, and data used to classify the alerts are shown in between dashed vertical lines (30-day-history data are attached with the alert). The alert leading to the KN trigger, *ZTF21abqfzcp*, was emitted on 2021-08-03 08:51:48 UTC. On the next re-observing night (five days after), new photometric data from alerts favoured a supernova candidate classification, ruling out the nature of the transient being a KN.

flux, residuals, and the number of measurements. Because we have better accuracy with more principal components, choosing the number of principal components is a compromise between the efficacy of the classifier and the amount of time that is needed to classify alerts and identify candidates (the more components, the more measurements we need, see Biswas et al., in prep. for more details).

In the early days of the campaign, we were using only the first principal component. However, it was shown quickly that one component was not sufficient to produce a reliable score on the alert data, and we had many false-positives (e.g., many candidates were obvious supernovae). So we introduced the second principal component in the set of features for the classification, and the results with real data improved without introducing further delays in practice given the cadence of the ZTF survey (that is without the need to add more measurements). In addition, the average number of candidates per month was reduced, from about 28 candidates per month to about 10 per month. The change of the model in the classifier happened on 17 June, 2021. In FINK, data and model are versioned, and the new model corresponds to the version 0.4.5.

This filter uses the five following criteria:

- The score from the KN classifier must be above 0.5 (binary random forest classifier).
- Point-like object: the star/galaxy extractor score must be above 0.4.
- Non-artifact: the deep real/bogus score must be above 0.5.
- Object not referenced in the SIMBAD database (except from extra-galactic origin).
- Young detection: less than 20 days. This threshold is quite loose but it is sufficient to filter long-trend or well-known objects.

Over the campaign, this filter selected 107 alert candidates out of 12,556,539. This corresponds to 70 unique objects on the sky (the same astrophysical objects can emit several alerts over time). Fig. 3 shows the light curve of such a candidate. All objects are labeled in the FINK database and can be easily accessed via the Science Portal⁵, or via the REST API.

With time, FINK collects more alert data, and has a clearer view on the nature of each object. At the end of the campaign, we found that most objects that emitted at least one alert tagged as KN candidates were deemed to be supernova candidates; however, some remained as KN candidates.

We also performed a crossmatch with the data from the Transient Name Server. Considering only the candidates from the first model (before June 2021), most of the candidates turned out to be Type Ia supernovae (41/71). However, after the model used to classify alerts changed, 29/36 of the candidates had no counterpart in the Transient Name Server (i.e., there was no follow-up), the others being identified as cataclysmic variables (6/36) or Type IIb supernovae (1/36).

3.2.2 Near-by Galaxy Catalogs (KN-Mangrove)

With the previous filter, KN-LC, we concluded that a minimum of two days from the first detection by ZTF is necessary to get a reliable score from the classifier and to identify candidates. According to KN models, two days after the compact binary merger, the signal will be fading or even too faint to be observed. So we developed a second filter to address younger detections. This filter uses the following criteria:

- Point-like object: the star/galaxy extractor score must be above 0.4.
- Non-artifact: the deep real/bogus score must be above 0.5.
- Object not referenced in the SIMBAD database (except from extra-galactic origin).
- Young detection: less than 6 hours.
- Galaxy association: the alert should be within 10 kpc of a galaxy from the Mangrove catalog (Berger 2014). The 10 kpc is empirical – we also tested different values. Above 10 kpc, we have a very large rate of contaminants. Below 10 kpc, we would potentially miss valid transients.
- Absolute magnitude: the absolute magnitude of the alert should be -16 ± 1 mag (in both g' and r' bands).
- Non Solar System Object: the alert must be at least $5''$ away from any known Solar System objects referenced in the Minor Planet Center database at the time of emission.

With the KN-Mangrove filter, an alert will be considered as a candidate if one can identify a suitable host and the resulting absolute magnitude is compatible with KN models. To identify possible hosts, we used the MANGROVE catalog (Ducoin et al. 2020), containing about 800,000 nearby galaxies. For the campaign, we only considered galaxies within 230 Mpc, as it corresponds to the current observation

⁵ <https://fink-portal.org>

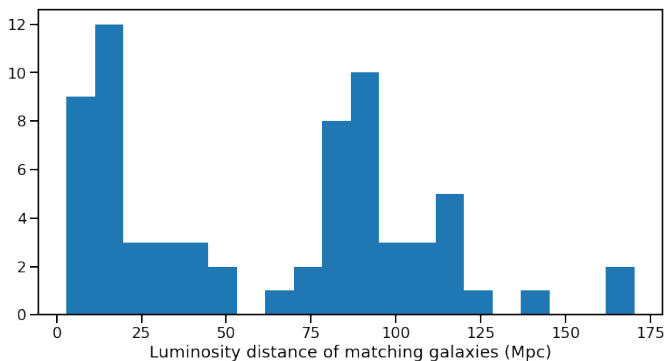


Figure 4. Histogram of the luminosity distance of galaxies associated with alerts selected by the KN-Mangrove filter. For the campaign, we only considered the galaxies from the Mangrove catalog in a 230 Mpc range, corresponding to the observation range of current GW detectors. In practice, we have no candidates further than 170 Mpc. Alerts and galaxies are matched within a radius of 10 kpc. The threshold has been set such to avoid a large number of spurious associations in the observation plane, while allowing coverage around the galaxy. Note that the allowed angular distance between alerts and galaxies increases when the luminosity distance decreases, hence leading to more frequent spurious associations at small luminosity distances.

range of GW detectors. Fig. 4 shows the distribution of luminosity distances of galaxies associated with alerts selected by the KN-Mangrove filter.

In practice, the galaxy association method is not perfect, and can lead to misassociation of an event that is in the foreground or the background of a galaxy⁶. But this is inevitable, as the luminosity distance between the Earth and the source generating the alert is usually unknown.

According to Kasliwal et al. (2020), we expect a KN event to have a peak absolute magnitude at $g' \sim -16$ mag. This threshold is given in g' -band, but in this work it was implemented for g' and R' bands without distinction. This hypothesis is due to the lack of early observations and strong consistency with AT2017gfo (Abbott et al. 2017b). As we often do not know the source distance, we compute the absolute magnitude from an alert as if it were in the matched galaxy.

68 alert candidates were selected by this filter out of 12,556,539 processed alerts from 01 April to 30 September, 2021. This corresponds to 59 unique objects on the sky. At the end of the campaign we checked, using more data, the evolution of the classification of those objects. We found that most objects remained KN candidates according to the KN-Mangrove classifier, while a small fraction were subsequently identified as potential supernova candidates or Solar System Object candidates. This was confirmed when checking against Transient Name Server data, where we found 51/68 alerts without a counterpart (i.e., no follow-up result

⁶ See for example <https://fink-portal.org/ZTF21abdwdwo> that was selected by the KN-Mangrove filter and associated with the bright LEDA 1740743 galaxy in Mangrove. After visual inspection, it turns out that the alert more likely originated from a fainter galaxy located further away, and not present in Mangrove.

was reported), 7/68 confirmed as supernova type Ia, 4/68 as supernova type II, 3/68 as supernova type IIp, 1/68 as supernova type IIb, 1/68 as supernova type Ib, and 1/68 as supernova type Ic.

3.2.3 Slope-based filter (KN-Slope)

In addition to the two previous filters, we developed a third filter based on the work of Andreoni et al. (2021b). The main criterion used for extracting KN candidates corresponds to the slope of the normalized light curve (mag/day). Given the expected light curves of KNe, we chose a threshold of 0.3 mag/day, which corresponds to a fast-fading object. This filter was not adopted during the campaign as it did not provide satisfying results. However for reference we reprocessed the campaign data and we present its performance here. This filter will be used in the subsequent campaigns along with the two other filters. In total, this filter implements eight criteria:

- Fast fade: The apparent magnitude decay rate of the alert must be above 0.3 mag/day in the last photometric band with two sequential measurements.
- Point-like object: The star/galaxy extractor score of the alert must be above 0.4.
- Non-artifact: The deep real/bogus score of the alert must be above 0.9.
- Object not referenced in the SIMBAD database (except from extra-galactic origin).
- Object not referenced in the Sloan Digital Sky Survey (SDSS) as a star or quasi-stellar object.
- Young detection: The alert emission date must be less than 14 days. In practice the delay between the first detection and the trigger by FINK is a maximum two days (two consecutive measurements by ZTF).
- Non Solar System Object: The alert must be at least 10'' away from any known Solar System objects referenced in the Minor Planet Center database at the time of emission.
- Away from the galactic plane: The alert must have an absolute galactic latitude above 10 degrees.

127 alert candidates were selected by this filter out of 12,556,539 processed alerts from 01 April to 30 September, 2021. This corresponds to 108 unique objects on the sky. At the end of the campaign, most of the objects had produced more alerts after the initial KN trigger, and were mostly falling under the class of supernova candidates according to the FINK filters. When cross-matching with data on the Transient Name Server, 117/127 have no counterparts, 6/127 are from cataclysmic variables, 3/127 are from supernovae type Ia, and 1/127 is from supernova type IIin.

3.3 Accuracy, efficiency, and added value

The main purpose of the classifier is to identify the most probable fast transient candidates in the sample, with a particular focus on KNe. However, to determine the nature of transients of interest, it generally requires follow-up photometry above and beyond what is provided by a survey with return timescales of ~ 1 night or more. For this reason, measurements of the number of transients passing the selection filters are required to understand the nature of objects that

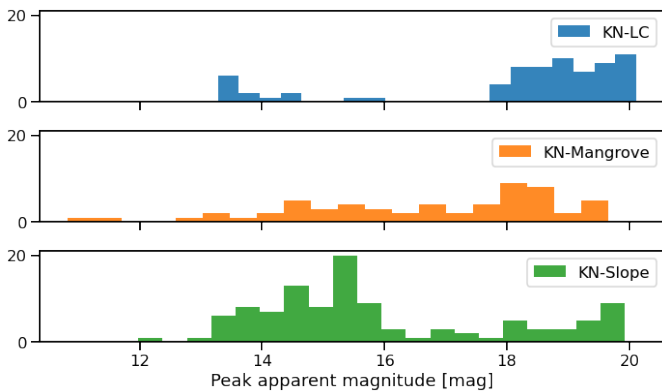


Figure 5. Histogram of the peak apparent magnitude for the candidates that pass the three filters: KN-LC (top, blue, see 3.2.1), KN-Mangrove (middle, orange, see 3.2.2), KN-Slope (bottom, green, see 3.2.3). In the case of the KN-LC and KN-Slope filters, the distributions have an excess of candidates at the two ends (faintest and brightest objects), while the peak apparent magnitude distribution in the case of KN-Mangrove is rather uniform across the magnitude range. The faintest peak apparent magnitude is around 20 mag for all filters.

will pass those filters. In particular, empirical measurements of the rate of transients passing particular filters are useful for assessing the contamination rate and therefore the follow-up photometry (and potentially spectroscopy) required to characterize the sample.

To evaluate the contaminant rate, we re-analyzed the ZTF alert stream data taken between November 2019 and September 2021 (538 observing nights), corresponding to 38,372,852 (12,149,579) processed alerts (unique objects). Using this data, 197 (132) alert candidates have passed the KN-LC filter, 227 (208) candidates passed the KN-Mangrove filter, and 285 (247) candidates passed the decay rate filter (KN-Slope). According to Transient Name Server classification data, for the KN-LC and KN-Mangrove filters, the most common contaminant transients were supernovae near peak⁷, and for the decay rate filter, the most common transients were fading cataclysmic variables near the Galactic plane. Given the ZTF coverage, this corresponds to a magnitude-limited rate of about 0.5 candidates per night per filter down to a magnitude of 20.5. Fig. 5 shows the histogram of the peak apparent magnitude for the candidates that pass the filters. While the KN-LC and KN-Slope distributions seem bi-modal (due to, for example, the excess of cataclysmic variables in the KN-Slope filter), the results from the KN-Mangrove filter are more spread across the magnitude range. Our analysis provides important information to understand the underlying population of contaminants (assuming there are no KNe) and also for future surveys as Vera Rubin LSST.

⁷ Note that in the case of KN-Mangrove, we would have four times more candidates if we did not reject Solar System objects.

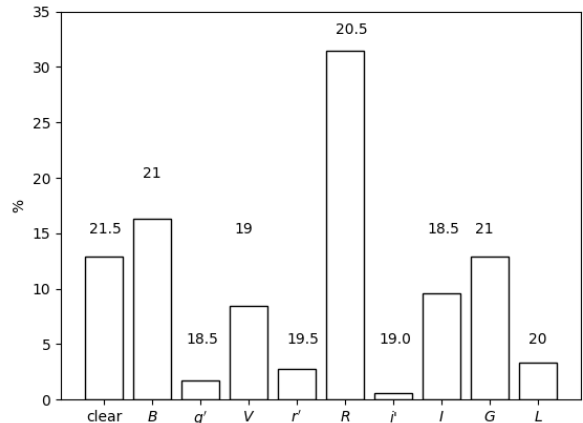


Figure 6. Filters used in the images taken during this observational campaign and when a source is detected. Above are mentioned the fainter upper limits reached during the campaign (see section 4.1).

4 GRANDMA/KILONOVA-CATCHER R04

We organized the “ready for O4 campaign-I” to a) demonstrate the potential of amateur astronomy in the search of GW counterparts, b) introduce the GRANDMA consortium into the search for KNe, and c) establish the caveats for performing joint photometry with different apertures and filters. From 21 May, 2021 to 21 September, 2021, we followed six alerts sent by our KN broker implemented in FINK (see section 3) focusing on alerts sent on Friday. The aim was to invite amateurs to observe the transient during the next 72 h (so that the amateurs would have the weekend for performing observations), to verify how many would respond and with which latency. If no alert passed our thresholds, we provided the observers recent supernovae (three in our campaign) to be observed for practice purposes. In July 2021, we invited all GRANDMA teams to observe kilonova candidates as well in order to have a larger set of images to test our photometric pipeline on heterogeneous data. Several online tutorials were organized allowing us to enroll a large number of amateurs with their respective observatories. A preliminary requirement file was released to indicate to the observers how to provide useful data for the campaign. In particular, we were firstly targeting a “classification mode” requiring the use of several photometric bands to either confirm the event detection or reject it as a false alarm, and secondly a “monitoring mode” by following up the multi-band flux evolution of the transient source.

In total, we achieved participation by 26 amateurs and 11 distinct GRANDMA telescopes (see Table 2). We received images taken with filters in professional and amateur filter systems, and also images taken without filters (see Figure 6).

4.1 Data reduction

In order to uniformly process the diverse set of images acquired by various telescopes, we developed two dedicated

photometric pipelines: STDPIPE⁸ (will be referenced henceforth as “STD”) and MUPHOTEN⁹ (Duverne et al. 2022) (will be referenced as “MU”).

STDPipe – STDPIPE (Karpov 2021) is a set of Python routines for astrometry, photometry and transient detection related tasks, intended for quick and easy implementation of custom pipelines, as well as for interactive data analysis. It is designed to operate on standard Python objects: NumPy arrays for images, Astropy Tables for catalogs and object lists, etc., and conveniently wraps external codes that do not have their own Python interfaces (SExtractor (Bertin & Arnouts 1996), SCAMP (Bertin 2006), PSFEx (Bertin 2011a), HOTPANTS (Becker 2015), Astrometry.Net (Lang et al. 2010), etc). It supports the following steps of processing and analyzing the images:

- object detection and photometry using either SExtractor (Bertin & Arnouts 1996) or SEP (Barbary 2016) codes. Simple PSF photometry may be performed by the SExtractor backend using a PSF model estimated by the PSFEx (Bertin 2011b) software, or aperture photometry based on photutils (Bradley et al. 2021) may be run using various kinds of background estimation, either global or local.

- astrometric calibration using Astrometry.net (Lang et al. 2010) for blind World Coordinate System (WCS) solving in either remote or locally-installed variants, and using SCAMP (Bertin 2006) or custom Astropy-based code for astrometric refinement by matching the lists of objects detected in image with catalog entries

- photometric calibration using any catalog available in Vizier as a reference with approximate on-the-fly passband conversion for some of them (in order to derive the magnitudes in the Johnson-Cousins system based on the ones in Pan-STARRS or Gaia systems). A sophisticated photometric matching routine is available for fitting the zero point and photometric system of the frame taking into account a spatial polynomial of arbitrary order, a color term, as well as an optional additive flux term.

- image subtraction with the HOTPANTS (Becker 2015) code using either locally available templates or images automatically downloaded from the network. The code allows downloading templates either from the Pan-STARRS archive of stacked images (Waters et al. 2020), or from any imaging survey accessible through the HiPS2FITS (Boch et al. 2020) service. When running the image subtraction code, a custom noise model may be supplied in order to account for the poorly known gain and bias levels of the image.

- transient detection and photometry on difference images taking into account the proper noise model of the difference image and various artifact masks in order to decrease the number of false detections. The transients may be filtered based on coincidences with either locally available or remote catalogs, as well as with positions of known Solar System objects. Also, optionally a routine for sub-pixel adjustment of the transient cutout and template images may be performed in order to detect cases of slight positional shifts (causing “dipoles” in difference images) either due to

overall image misalignment, or object proper motion due to a large difference in the template epoch.

- insertion of simulated stars with realistic PSFs into the images in order to assess the performance of transient detection.

- the code also includes various convenience utilities and plotting routines for quick visualization of the results of every step.

The actual image processing pipeline for the present work was organized as follows. As STDPIPE is intended for higher-level analysis of pre-processed frames, we required all images to be pre-processed by an instrument-specific code to perform bias, dark subtraction, and flat-fielding in advance. Then we removed the cosmic rays using the astrocrappy (McCully & Tewes 2019) code implementing the original LACosmic (van Dokkum 2001) algorithm, and detected the objects on the image using SExtractor (Bertin & Arnouts 1996). Next, we performed aperture photometry with local background subtraction using a photometric aperture with radius equal to the median image full width at half maximum (FWHM), and a background annulus between radii of 5 and 7 FWHM units. Then, the astrometric solution was derived using the Astrometry.net (Lang et al. 2010) solver applied to the list of detected objects. Then, we downloaded the list of stars from the Pan-STARRS DR1 catalog from Vizier to serve as both an astrometric and photometric reference catalog, and augmented it with Johnson-Cousins B , V , R_C and I_C magnitudes using approximate conversions derived by Kostov & Bonev (2018). We refined the image astrometric solution using the SCAMP (Bertin 2006) code, via lists of detected objects and catalog stars. Then we constructed the photometric solution for the image using the closest Johnson-Cousins filter as a reference and $B - V$ (or corresponding Pan-STARRS filter and $g' - r'$ for the telescopes using Sloan-like filter sets) as a color used for deriving an instrumental photometric system (color term). For the zero point, we used either a constant value for all stars if the field of view (FOV) and number of stars were small, or a second order spatial polynomial if there were enough stars in the frame. Then we downloaded the Pan-STARRS co-added images covering the observed field of view in the closest filters (either g' , r' or i'), mosaiced them and used the result as a template which was then subtracted from the image using the HOTPANTS (Becker 2015) code. On the resulting difference image, we performed forced aperture photometry at the transient position using the same settings as used for deriving the original photometry, so that the zero point model was still valid, and thus derived the transient photometry in a system linked to a standard one (either Johnson-Cousins or Pan-STARRS) by a color term value specific for this frame. In a similar manner, we determined an effective detection limit at the transient position by converting the background noise inside the aperture multiplied by 5 (so that it corresponds to 5σ) to flux and then to the magnitude. When the object is not detectable in the image, this value was adopted as an upper (detection) limit for its magnitude.

MUphoten – MUPHOTEN (Duverne et al. 2022) is a Python-based software dedicated to photometry of transients followed up by heterogeneous telescopes. It uses public Python libraries such as Photutils (Bradley et al. 2021), Astroquery (Ginsburg et al. 2019), and also uses external C

⁸ STDPIPE is available at <https://gitlab.in2p3.fr/icare/stdpipe>

⁹ MUPHOTEN is available at <https://gitlab.in2p3.fr/icare/muphoten>

codes: SExtractor (Bertin & Arnouts 1996), Scamp (Bertin 2006), Swarp (Bertin et al. 2002) and HOTPANTS (Becker 2015). The pipeline works on pre-processed images (dark or bias subtracted, flat-fielded) and for which an astrometric solution is known. For this campaign the astrometric calibration was done directly on the Astrometry.net website (Lang et al. 2010). The analysis process works as follows:

- subtraction of a Pan-STARRS template constructed with a mosaic of the observed FOV downloaded from the catalog archives. For non-Sloan filters (e.g., Johnson-Cousins or unfiltered images), the closest band of the Pan-STARRS system was used: g_{ps1} for B , V and clear images, r_{ps1} for R_C images, and i_{ps1} for I_C .

- background estimation in a mesh of 150×150 pixels, using the same estimator as SExtractor. The background is then subtracted from the image.

- source detection using a 2σ threshold above the background.

- aperture photometry on the detected sources.

- cross-match with Pan-STARRS catalog to fit the instrumental magnitude versus Pan-STARRS magnitude relation with a linear fit. For images acquired using filters of the Johnson-Cousins photometric system, we used the second order equations 1, 2, 4 and 6 of Table 2 from Kostov & Bonev (2018) to transform the Pan-STARRS system to the observed filter. For clear images, we added the flux from the g_{ps1} and r_{ps1} Pan-STARRS bands.

- detection of the transient in the residual image between the observed and the template images, adopting a 3σ threshold. A positive detection of a transient was considered if a source was identified at less than five pixels from the transient position.

- evaluation of the transient instrumental magnitude in the residual image between the observed and the template image from the Pan-STARRS survey and usage of the previous fit to obtain the calibrated measurement of the transient.

MUPHOTEN uses two methods to filter out poor quality images. One by comparing the calibrated magnitude of a star in the field of view to its magnitude in the catalog used for the photometric calibration. If they are incompatible, the image is rejected. The second veto consists in computing the seeing of the image with PSFex (Bertin 2011a). Then for a given band of a given telescope+filter configuration, reject the images for which the seeing deviates by more than 3σ from the median seeing of the data set. For the images passing the vetoes with no detected transient, we set an upper limit on the magnitude. It is estimated by dividing the number of detected objects in the image by the number of objects in the reference catalog in magnitude bins. When the result drops below 0.5, the center of the corresponding bin is considered to be the limiting magnitude.

4.2 Consistency of the analysis

We processed the images using both the STDPIPE and MUPHOTEN pipelines, thus acquiring two independent sets of measurements based on different photometric models – the one with a color term for the former, and without it for the latter. While the former is more accurate in theory, it requires the knowledge of a true transient color at the time of measurement in order to convert the result to standard

Table 3. Summary of the difference $\text{mag}_{MU} - \text{mag}_{STD}$ used for image reduction, separated by filter.

Band	Mean difference [mag]	standard deviation [mag]
B	0.2	0.2
V	< 0.1	0.1
R_C	-0.1	0.2
I_C	< 0.1	0.2
g'	< 0.1	0.1
r'	-0.01	0.1
i'	0.1	0.1
Clear/L	-0.4	0.3

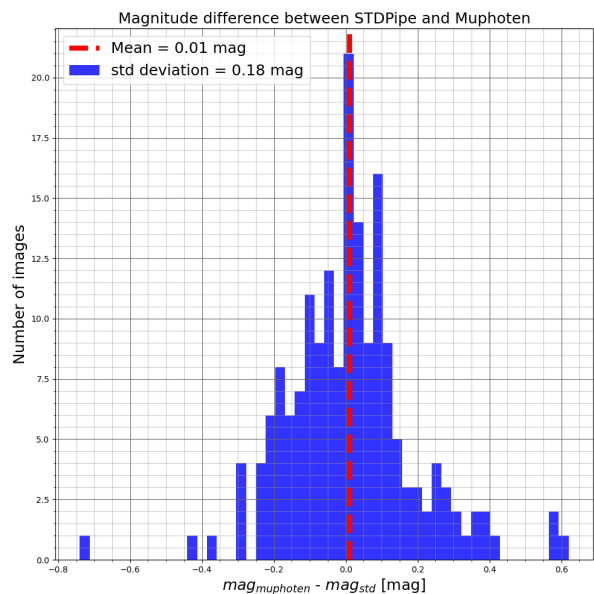


Figure 7. Distribution for difference in magnitudes for all the images where the transient is detected, but the unfiltered ones.

photometric system. As we, in general, do not always know it, for the sake of current analysis we decided to ignore the contribution from color terms and assume the color (either $g' - r'$ or $B - V$, whatever has been used for the photometric calibration of individual frames) to be the zero. This introduces a systematic color-dependent error for the two methods to the results of photometry. In order to assess the error, as well as other possible sources of bias, we compare the results of the two different methods in Figure 7 for all the images where the transient is detected, except for the clear ones and ones using a luminance filter. The latter correspond to a band covering the optical domain from UV to NIR, and is denoted L band in the next sections. The mean difference between STDPIPE and MUPHOTEN magnitudes for these images is less than the 0.1 mag, which is the typical uncertainty of the measurements. Thus, on average the difference between the results of the two pipelines is compatible with zero and the width of the distribution (0.18 mag) is comparable to the typical accuracy of each measurement, and so we can conclude there are no biases.

4.3 Rapid linear fit and offline classification

A “detection” corresponds to the first **public** photometric detection of ZTF (defined as T_0). Images are grouped with 0.1 day precision. A group contains at least one image.

Linear fit method – Our goal was to identify transients undergoing rapid decrease or increase in brightness. We applied a linear regression procedure using a maximum likelihood estimation approach to estimate the slopes between two different time bins, $t_i = T_0 + n_i$ days, where $n_i = 0.1 \times i$, and i is the index of a given time bin (see Appendix B). The slopes of the best fit, $a_r(t = n)$, are then computed using data taken with r or R filters in a given time bin. We actually computed three slopes:

(i) $a_{\text{STD},r}(t = n)$, the temporal slope of the transient light curve between the first detection by ZTF at T_0 and the time at which GRANDMA detected it by using STDPipe.

(ii) $a_{\text{MU},r}(t = n)$, the temporal slope of the transient light curve between the first detection by ZTF at T_0 and the time at which GRANDMA detected it by using MUphten.

(iii) $a_{\text{ZTF},r}(t = n)$, the temporal slope of the transient light curve between the first detection by ZTF at T_0 and the next detections by ZTF.

Offline source modeling - to constrain the nature of rapidly evolving optical transients using four light curve models a posteriori. For each of these models, we evaluate its degree of correlation with the observational data. We will use a KN model taken from Kasen et al. (2017) (Ka2017), a GRB afterglow (TrPi2018, Troja et al. 2018), the nugent-hyper model which creates supernovae light curve (nugent-hyper, Levan et al. 2005) and a shock cooling supernova light curve model (Piro2021, Piro et al. 2021). The ideal model is one that has a regression consistent with the light curve points as assessed by the Bayes factor of the model.

4.4 Results

In the following section, we summarize our observations and analyze the results produced by both STDPipe and MUphten to extract information about the nature of the transients (see Figure 8). We use MUphten for evaluating the upper limit of the image when no source has been detected by both pipelines independently. If the two pipelines provided inconsistent results for an image that had not been previously rejected, we excluded it from further analysis. Some GRANDMA teams performed their own measurements, but in order to keep a consistent analysis, they are not presented in this article. All our results are presented in Table A2.

4.4.1 KN-Mangrove alert candidates

ZTF21abdwdwo was observed by eleven amateur telescopes with a total of 42 images taken from 0.7 days to 9 days after the public detection (021-06-04 04:27:26 UTC) (see Table A1). The associated alert was sent by FINK without any further delay. All images resulted in non-detections with a median upper limit of 17.9 ± 0.8 mag in the r' and R -band filters. An unfiltered image taken by the T40-A77DAU telescope 0.8 days post-detection yielded a 20.7 mag limit. T-CAT obtained the deepest upper limit (~ 21 mag in B - and

G -band) 3.7 days post-detection (2021-06-07 21:41:04). At a much later date, the VIRT telescope confirmed the previous non-detections on 2021-08-03, 60 days post-detection with an upper detection limit of $R = 17.5$ mag. Our refined analysis showed there was a misassociation of the new source and the possible galaxy (see section 3.2.2). In summary, GRANDMA follow-up classified the new source as a Solar System Object 0.8 day after ZTF discovery.

ZTF21abfmbix (later renamed SN 2021pkz, associated with the galaxy 2MASS-12551554+0253477 at 38 Mpc) was observed by 13 different amateur telescopes and FRAM-Auger with a total of 29 images taken between 0.7 and 50.8 days after T_0 (2021-06-11 05:14:49). The associated alert was sent by FINK with a 1.5 hour delay. Two days before, ZTF did not detect any source brighter than $g' > 20.5$. A positive detection was found in 24 of the 29 images, using both the STDPipe and MUphten pipelines. These images were taken in six different filters and also with no filter from 0.7 days to 29.7 days post-detection. The next public ZTF measurement ($g' = 17.1$ mag, $r' = 16.9$ mag) was delivered two days after the first detection. We note that 17 of 25 photometric measurements (68%) delivered from STDPipe and MUphten are consistent within 0.1σ . We also note a maximum deviation of 0.6 mag in the L band and for images taken with no filter, when comparing the results of both pipelines. According to the results obtained with both pipelines, the data clearly show a transient in rising phase in the r' band. We evaluated the slopes of the luminosity rate (see Section 4.3) as: $a_{\text{STD},r}(t = 0.7) = -0.7 \pm 0.2$ mag/day and $a_{\text{MU},r}(t = 0.7) = -0.9 \pm 0.2$ mag/day. While the luminosity rate estimations differ between STDPipe and MUphten, it is clear that the source is brightening. We also found agreement between the slope of the luminosity rate using the different pipelines for $t = 1.7$ (-0.5 ± 0.1 and -0.7 ± 0.1 mag/day for STD and MU, respectively), and the value obtained from the public data at $t = 2.0$ days ($a_{\text{ZTF},r} = -0.5 \pm 0.1$ mag/day). This example shows the benefit of advanced measurements (+16 h first estimation, and 40 h confirmation) during the rising phase of the transient, and this will be useful for any decision on spectroscopy observations before night-time in the Americas. This depends on our capacity to promptly analyze the data as soon as it is acquired. A two-day long rise in the r' band is atypical for standard KNe at 38 Mpc and could only be related to very particular ejecta configurations during a NS-BH collision (Bulla 2019). Also, we note an independent spectroscopic measurement by the ZTF Spectral Energy Distribution Machine (SEDM) on $T_0 + 0.1$ days, classifying the source as a **supernova Ia**.

ZTF21abultbr was observed by three amateur telescopes and by the Abastumani-T70, providing a total of eight images from 0.6 day to 2.5 days after T_0 (2021-08-21 02:44:39.100 UTC). The associated alert was sent by FINK with a 10 minute latency with respect to the public detection. The source was presumably associated with HyperLEDA/UGC04104, located at 89 Mpc. Three of the eight images, taken with two different telescopes, led to a positive detection of the object using the STDPipe and MUphten pipelines. These images were taken with in R and G bands, and also with unfiltered observations. The next public ZTF measurement ($r' = 18.7$ mag) was delivered three days after the first detection of the source. We note the consis-

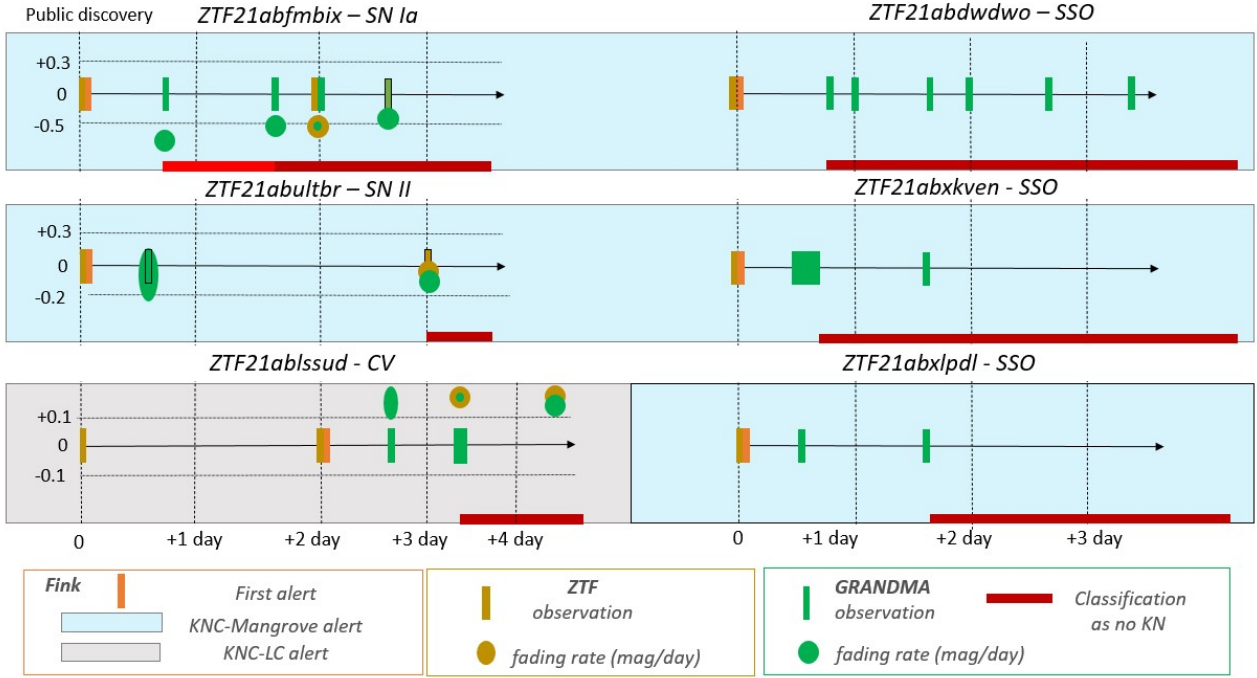


Figure 8. Overview of the GRANDMA observations of the six ZTF-Finkalerts followed up by professional and amateurs astronomers. The ZTF-Finkalerts came from two selection filters of the initial ZTF flux measurements named “KN-LC” and “KN-Mangrove” (see section 3). Displayed in orange are the time-stamps for the first alert provided by FINK Gold vertical bars represent the time-stamps of the release of ZTF public data, and green vertical bars represent the GRANDMA data analyzed by STDPipe and MUPhoten. The circles present our fading slope estimation using r'/R filters (see section 4.3); in gold using only ZTF public data, and in green using ZTF+GRANDMA data. Horizontal red bars show the period when the alert is considered as of no further interest for KN searches. SSO corresponds to Solar System Object, CV to cataclysmic variable, and SN to supernova given by our post-observation analysis months after (see figure 4.4.4). We see the potential of the amateur community to distinguish astrophysical events into three categories: moving objects, fast transients (KNe, GRBs) and slow transients (supernovae, CVs).

tency of photometric measurements between STDPipe and MUPhoten, except for images taken with no filter. At $t = 0.6$ day, the luminosity rate (see Sect. 4.3) exhibits the following slopes: $a_{STD,r}(t = 0.6) = -0.2 \pm 0.4$ mag/day and $a_{MU,r}(t = 0.6) = -0.0 \pm 0.4$ mag/day. The value obtained from the public data at $t = 3.0$ days ($a_{ZTF,r'}(t = 3.0) = -0.0 \pm 0.1$ mag/day). These measurements were insufficient to conclude the nature of the transient and how it evolved from 0.6 to 3.0 days. The monitoring of the source by ZTF was interrupted between $t = 3.0$ to $t = 21.0$ days. The source was independently classified as a [supernova II](#) after 21 days by the ZTF SEDM.

[ZTF21abxkven](#) was observed simultaneously by the Abastunami/T70, TRT-SRO, Lisnyky/Schmidt-Cassegrain, and FRAM-CTA telescopes, as well as nine different amateur telescopes with a total of 17 images taken between 0.5 and 11.7 days after T_0 (2021-09-03 08:28:07). It was presumably associated with [HyperLEDA- UGC12816](#) located at 80 Mpc based on the KN-Mangrove filter. The associated alert was sent by FINK without any further delay. With no more alert data sent for this location on the sky, FINK classified this transient independently as a Solar System object (Möller et al. 2020). All images resulted in non-detections with a median upper limit of 20.6 mag in underfiltered im-

ages within the first day of observation. A clear image (no filter) was taken at 0.7 day after T_0 by T-ST SOPHIE, with a 20.6 mag upper limit. In summary, the GRANDMA follow-up ruled out any possible existing KN within 80 Mpc at $T_0+0.7$ day.

[ZTF21abxlpdl](#) was observed simultaneously by the Abastunami/T70, FRAM-CTA, and TRT-SRO telescopes, as well as seven amateur telescopes. A total of 15 images were taken from 0.5 to 13.9 days after the first public detection (2021-09-03 08:59:15). The alert was sent the same day as ZTF21abxkven, so the participation was limited for both targets. The transient was presumably associated with NGC 105, located at 79 Mpc based on our KN-Mangrove filter. The associated alert was sent by FINK without any further delay. All images resulted in non-detections with a median upper limit of 20.0 in unfiltered observations (see some examples in Table A1). A clear image was taken 1.7 days after the alert using the T40-A77DAU, with an upper limit estimated at > 20.7 mag. In summary, the GRANDMA follow-up ruled out any KN within 80 Mpc at $T_0+1.7$ day with luminosity decay rate < 1 mag/day in the r' band. Some scenarios involving both BNS and NSBH collisions can produce steeper decay rates > 1 mag/day in the r' band, although these cases are extremely rare (see Bulla 2019).

4.4.2 KN-LC alert candidates

[ZTF21ablssud](#) was observed simultaneously by the TRT-SRO, Lisnyky/Schmidt-Cassegrain, Tibet-50, and UBAINT60 telescopes, as well as 17 different amateur telescopes, leading to a total of 141 images taken between 2.6 to 26.7 days after T_0 (2021-07-16 21:11:45). The associated alert from the KN-LC filter was sent by FINK two days after the discovery with a probability of 53% classification (see section 3.2.1). Other scores were delivered by FINK Early SN (5%), Supernova SN Ia vs non-IA SN (73%) and SN Ia and Core-Collapse vs non-SN (39%). Observations started 0.6 days after the FINK alert. A total of 66 images taken with eight different filters (and additional unfiltered images) from 17 telescopes exhibited a positive detection of the object using both the STDPipe and MUphoten pipelines. The next public ZTF measurement post-FINK alert ($r' = 17.2$ mag in the r' band) was delivered five days after the first detection. For $t = 3.7$ days, we derived the slope of the luminosity decay rate (section 4.3) as 0.15 ± 0.1 mag/day for both STDPipe and MUphoten. The slopes obtained from the ZTF public data are $a_{ZTF,r} = 0.15 \pm 0.1$ mag/day at $t = 2.0$ day and $t = 5.0$ day. We ruled out the association with a standard KN resulting from the coalescence of two binary neutron stars. No spectra have been reported in the literature. FINK scored the transient as Supernova (79%) after 30 days of observations by ZTF. GRANDMA accumulated an important collection of data for $t < 10$ days compared to the available data in the literature (see Figure 9). Based on the color evolution and the location of the source close to the galactic plane, we proposed that the source corresponds to a cataclysmic variable event. In addition, the light curve fitting of ZTF data ruled out the nature of the source as a KN, GRB afterglow, or supernova event (see section 4.4.4).

4.4.3 Training alert candidates

Here, we briefly describe our observations on “training alerts” distributed by FINK. The alerts are produced via different channels: supernova and KN candidates. They were not only scheduled for Fridays and were proposed for observing on a best-effort basis by the FINK team for practice.

[ZTF21abfaohe/SN 2021pfs](#) and [ZTF21abbzjeq/SN 2021mwb](#) were classified as supernovae (see TDS for external reference and section 4.4.4). [ZTF21abotose/SN 2021ugl](#) is a supernova IIB. The three sources distributed via FINK were selected to test the data reduction capabilities of GRANDMA. Photometric results are reported in Appendix A.

[ZTF21abyplur](#) was only observed by the Tibet-50 with four images beginning 9.5 days after the first public detection reported on 2021-09-07 09:12:26. The associated alert was sent by FINK without any further delay but the amateur astronomers were not notified because it was outside of our Friday exercise. The alert-host association (HyperLEDA-PGC1115282) is within $10''$, almost at the limit of a positive association; it might have been incorrectly associated with the galaxy. FINK classified this object independently as a Solar System object, probably attached to Solar System object number 22327 (Möller et al. 2020). The images taken by the Tibet-50 could not rule out the case of a fast transient with an upper limit of $g' > 18.3$ mag, at $t = T_0 + 9.5$ days.

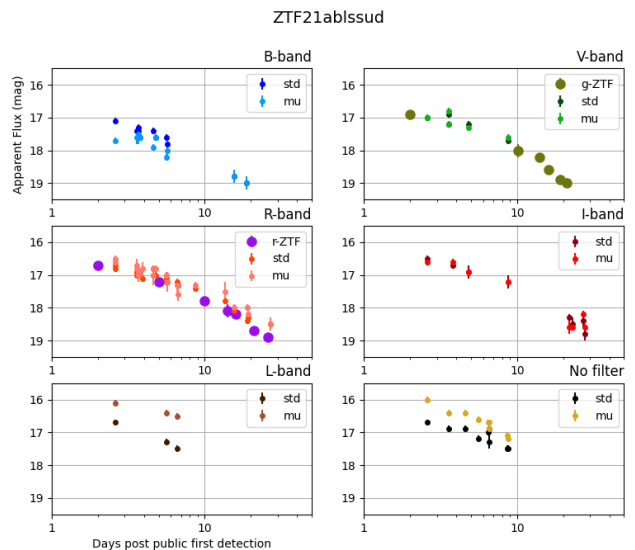


Figure 9. ZTF21ablssud light curves with ZTF as well as the GRANDMA observations from 17 different telescopes. The data were mostly taken by amateur astronomers before $t = T_0 + 10$ days, and by professionals for $t > T_0 + 10$ days. STDPipe and MUphoten measurements are in agreement for V , R_C , and I_C bands. In the L filter as well as in unfiltered images, MUphoten adds flux from g' - and r' -band Pan-STARRS images while STDPipe treats them as R_C -band images. We show that the GRANDMA measurements are consistent with the ZTF ones, allowing for filling in the light curve gaps. However the use of non-standard filters by some amateur astronomers (especially the B band of the T-CAT instrument) can lead to discrepancies between measurements up to 0.5 mag.

[ZTF21absvlrr](#) was observed by six amateur telescopes and the Terskol/Zeiss-600, TRT-SBO, TRT-SRO, and Abastumani-T70 telescopes, leading to a total of 24 images taken from 1 to 59 days after T_0 (2021-08-12 09:52:43). The associated alert from the KN-Mangrove filter was sent by FINK with a 2.3 hour delay, but distributed to GRANDMA as a practical exercise about 0.9 days afterwards. The source was presumably associated with [HyperLEDA/ESO540-025](#) located at 89 Mpc. A total of 19 images taken with seven telescopes confirmed a positive detection of the source using both STDPipe and MUphoten pipelines. These images were taken in B , V , r' , R , as well as unfiltered. The next public ZTF measurement ($g' = 17.6$ mag, $r' = 17.7$ mag) was delivered two days after the first detection. We note the consistency of photometric measurements between STDPipe and MUphoten, except for images taken with no filter. According to the results obtained with both pipelines, the data clearly shows a transient in the rising phase in the r' band, based on the slopes of the light curves at $t = 1.0$ day (-0.1 ± 0.2 mag/day for both STD and MU), and at $t = 1.7$ days (-0.5 ± 0.1 and -0.7 ± 0.1 mag/day for STD and MU, respectively). At $t = 2.0$ days, the slope obtained from the ZTF public data is $a_{ZTF,r} = -0.5 \pm 0.1$ mag/day. In addition, we also observed a two-day long rise of the source in B (-0.7 ± 0.2 and -0.8 ± 0.2 mag/day for STD and MU, respectively, at $t = 2.0$ days) and in the g' -

band ($a_{\text{ZTF,g}}(t = 2.0) = -0.6 \pm 0.1$ mag/day). The source, at an early stage, did not behave in a manner similar to AT2017gfo. We note an independent spectroscopic measurement by the ZTF SEDM on $T_0 + 1$ day, classifying the source as a [supernova Ia](#).

ZTF21acceboj/SN 2021yyg was only observed by Tibet-50 and Terskol-600 telescopes with a total of 11 images taken after 1.4 days from the first public detection reported on 2021-09-14 11:04:25. The associated alert from the KN-Mangrove filter was sent by FINK without any further delay but the amateur astronomers were not notified since it was out of our Friday triggering schedule. From linear regression fitting (see section 4.3) we obtained $a_{\text{STD},r}(t = 1.4) = -0.3 \pm 0.1$ mag/day, and $a_{\text{MU},r}(t = 1.4) = -0.4 \pm 0.1$ mag/day. Using public data we measured $a_{\text{ZTF},r}(t = 2.0) = -0.3 \pm 0.1$ mag/day. The source clearly exhibits a two-day rise in the r' band that ruled out ZTF21acceboj as a KN stemming from the coalescence of two binary neutron stars. The Global SN Project (with LCO) classified the source as a [supernova IIp](#) one day after than the first public detection.

4.4.4 Constraining the nature of transients with offline results

The objective of the “ReadyforO4” campaign was to gather information on the nature of transient events and their evolution. Events were followed during weekends, but not monitored over several weeks. Hence our GRANDMA sample covered essentially two epochs: when the alert was received by our amateur astronomers, and when the professional telescopes joined the campaign in July. In this sense, we trained our team on the ZTF data available to confirm the nature of the sources we followed up with GRANDMA using models described in section 4.3. The ZTF data are used to validate the models by generating the logarithm of the Bayes factor, the level of correlation of the model fit with the data, and increase our knowledge of the physical processes following the observation.

In Table 4, we present the results obtained for each transient clearly identified as a non-moving object through the analysis of the light curve from ZTF data. Using the models described above, we identify ZTF21abfmbix, ZTF21absvlrr, ZTF21abultbr, ZTF21abfaohe, ZTF21abfmbix, ZTF21abbzjeq and ZTF21acceboj as typical supernova candidates. ZTF21abotose is both consistent with shock cooling and GRB afterglow models at early times. However, the increase of its brightness at later times is in good agreement with the shock cooling scenario only. ZTF21ablssud is well-fit by a GRB model, however, due to its galactic latitude ($\ell = 5.7$ deg) and similarity to many other examples of cataclysmic variables in the literature, it is likely a cataclysmic variable.

5 CONCLUSIONS

In this paper we describe GRANDMA’s “ReadyforO4” campaign to search for serendipitous KNe using ZTF public data filtered by FINK and followed-up with GRANDMA facilities. Eight objects in total were observed, using 26 amateur telescopes and eleven professional telescopes (34 of which

provided data analyzed in this work). Through FINK and follow-up, no KNe were identified, instead we classified four of these objects as asteroids, while the remaining were classified as cataclysmic variables and supernovae. In addition to demonstrating a number of challenges for observing transient sources with a variety of telescopes of different apertures, filters, and configurations, we achieved a number of successes.

- **Reaction time** – We obtained the first images from the amateur community less than 16 hours after the FINK alert. This delay is due to the fact that most of our amateur community is located in Europe (especially in France). In the future we hope to connect with other amateurs across the world, although language barriers remain a challenge.

- **Data acquisition and filters** – The GRANDMA facilities are mostly equipped with red filters, which are excellent for the characterization of KNe events. Our campaign showed that amateur astronomers reached a depth of 21 mag with a variety of filter configurations. These astronomers will be an asset during O4, for which we might expect AT2017gfo-type KN events peaking at ~ 21 mag for events located at the observational horizon of the GW interferometers (Petrov et al. 2022). However, the use of filter sets (Johnson-Cousins, L -, w - and o -filters) different from those of the SDSS, which was our reference catalog for this analysis, remains problematic for the characterization of the sources. For this reason, we found that the use of two standard data reduction pipelines (STDPipe and MUPHOTEN) is a way to standardize results (as compared to allowing the individual telescope teams to reduce their own data). We observed a difference in magnitude of less than 0.2 mag for Johnson-Cousins and SDSS filters. Based on this experience, we would like to motivate our community to use only SDSS filters to have a homogeneous set of data. We also noted that images taken with no filter are particularly useful for guiding the observers for their data acquisition. We finally experienced miscommunication on products distributed to GRANDMA, as some observers provided pre-stacked images while others were submitted as individual images. This greatly reduced our ability to analyze the images at low latency, and so correcting this will be a focus for future campaigns.

- **Quality of the data sample** – Among the eight transients, a total of 450 images were taken by GRANDMA partners. However, we detected a source and were able to perform astrometry and photometry on only 180 images (40%). To improve this efficiency, we need amateur astronomers to gain expertise in their data acquisition and validation before distribution to the network. For example, some data had artifacts and “star” tracks, blur, or galaxy saturation that could easily be identified with more experience. Another challenge was the dispersion of format and keywords employed in the files, which slowed down our analysis. This will be partially solved in future runs with a set of required keywords, including the time of the start of the observation, the name of the telescope, the filter used and the filter system.

- **Classification** – We demonstrated the potential of the amateur community to distinguish astrophysical events into three categories: moving objects, fast transients (KNe, GRBs) and slow transients (supernovae, CVs). We based our rapid fast transient classification on the decay rate of the optical sources, which should reach a maximum of at

Table 4. Results of the simulations of transients with rapid evolution, in order to validate or reject the concordance of each transient using ZTF data with the four models: KNe (Ka2017), supernova (nugent-hyper), GRB afterglows (TrPi2018) and shock cooling (Piro2021). Note that the Bayes factors are evaluated logarithmically.

Transients	Ka2017	TrPi2018	nugent-hyper	Piro2021	light curve
ZTF21abfmbix	-12.38	-15.95	-9.18	-10.1	Supernova Ia
ZTF21absvlrr	-9.78	-16.73	-9.91	-11.07	Supernova Ia
ZTF21abultbr	-2.73	-9.14	-5.24	-4.76	Supernova II
ZTF21ablssud	-6.32	-11.58	-9.83	-9.41	Cataclysmic Variable
ZTF21abfaohe	-12.3	-10.98	-7.47	8.67	Supernova Ia
ZTF21abbzjeq	-8.22	-11.41	-7.49	-8.47	Supernova Ia
ZTF21acceboj	-16.52	-19.44	-14.52	-15.6	Supernova IIb
ZTF21abotose	-6.37	-10.62	-7.41	-7.49	Shock Cooling - Supernova IIp

least 0.3 mag/day for KNe. The images posted by the professional and amateurs observers within the first 2 days after the FINK alert helped to categorize the candidates, which were discovered at an average magnitude of $r'18.1 \pm 1.0$ mag. This classification improved on the timing relative to routine observations by ZTF during the American night. In addition, we also developed rapid and sophisticated modeling tools that can be applied to GRANDMA data during the O4 observing run. If we are able to run data reduction in near real-time, we would be able to filter the most probable candidates a few hours before the second night of observation in the Americas after a GW alerts. This will allow us to trigger spectroscopic observations with higher confidence during the O4 observing run, mitigating the use of valuable resources on non-viable candidates.

Overall, we consider the first “ReadyforO4” campaign to be a success which can be built upon to allow the amateur community to partake in cutting-edge astrophysical science once the fourth observing run of the LIGO-Virgo-KAGRA detectors begins in late 2022/early 2023.

DATA AVAILABILITY

The data underlying this article will be shared on reasonable request to the corresponding author.

6 ACKNOWLEDGEMENTS

SA and CL acknowledge the financial support of the Programme National Hautes Energies (PNHE). SA acknowledges the financial support of CNES. SA is grateful for financial support from the Nederlandse Organisatie voor Wetenschappelijk Onderzoek (NWO) through the VIDI (PI: Nissanke). SA dedicates her contribution to Rayan Ouram, who is a source of inspiration for bravery and humanity for GRANDMA. DT acknowledges the financial support of CNES post-doctoral program. UBAI acknowledges support from the Ministry of Innovative Development through projects FA-Atech-2018-392 and VA-FA-F-2-010. RI acknowledges Shota Rustaveli National Science Foundation (SRNSF) grant No - RF/18-1193. TAROT has been built with the support of the Institut National des Sciences de l’Univers, CNRS, France. MP, SK and MM are supported by European Structural and Investment Fund and the Czech Ministry of Education, Youth and

Sports (Projects CZ.02.1.01/0.0/0.0/16_013/0001403, CZ.02.1.01/0.0/0.0/18_046/0016007 and CZ.02.1.01/0.0/0.0/15_003/0000437). The FRAM telescope is also supported by the Czech Ministry of Education, Youth and Sports (projects LM2015046, LM2018105, LTT17006). NBO and DM acknowledge financial support from NASA MUREP MIRO award 80NSSC21M0001, NASA EPSCoR award 80NSSC19M0060, and NSF EiR award 1901296. PG acknowledges financial support from NSF EiR award 1901296. DAK acknowledges support from Spanish National Research Project RTI2018-098104-J-I00 (GRBPhot) XW is supported by the National Science Foundation of China (NSFC grants 12033003 and 11633002), the Scholar Program of Beijing Academy of Science and Technology (DZ:BS202002), and the Tencent Explorer Prize. The GRANDMA consortium thank the amateur participants to the *kilonova-catcher* program. The *kilonova-catcher* program is supported by the IdEx Université de Paris, ANR-18-IDEX-0001. This research made use of the cross-match service provided by CDS, Strasbourg. MC acknowledges support from the National Science Foundation with grant numbers PHY-2010970 and OAC-2117997. GR acknowledges financial support from the Nederlandse Organisatie voor Wetenschappelijk Onderzoek (NWO) through the Projectruimte and VIDI grants (PI: Nissanke). Thanks to the National Astronomical Research Institute of Thailand (Public Organization), based on observations made with the Thai Robotic Telescope under program ID TRTC08D.005 and TRTC09A.002. S. Leonini thanks M. Conti, P. Rosi, and L. M. Tinjaca Ramirez. SA thanks Etienne Bertrand and le “Club des Céphéides” for their observations of ZTF21abxkven.

REFERENCES

- Abbott B. P., et al., 2017a, *Phys. Rev. Lett.*, **119**, 161101
 Abbott B. P., et al., 2017b, *ApJ*, **848**, L12
 Alexander K. D., et al., 2017, *ApJ*, **848**, L21
 Almualla M., Coughlin M. W., Anand S., Alqassimi K., Guessoum N., Singer L. P., 2020, *MNRAS*, **495**, 4366
 Almualla M., et al., 2021, *Monthly Notices of the Royal Astronomical Society*, **504**, 2822–2831
 Andreoni I., Ackley K., Cooke J., et al., 2017, *PASA*, **34**, e069
 Andreoni I., et al., 2019, *PASP*, **131**, 068004
 Andreoni I., et al., 2021a, arXiv e-prints, p. arXiv:2106.06820
 Andreoni I., et al., 2021b, *ApJ*, **918**, 63
 Antier S., et al., 2020a, *MNRAS*, **492**, 3904
 Antier S., et al., 2020b, *MNRAS*, **497**, 5518

- Arcavi I., et al., 2017, *Nature*, **551**, 210
- Barbary K., 2016, *Journal of Open Source Software*, **1**, 58
- Bauswein A., Just O., Janka H.-T., Stergioulas N., 2017, *ApJ*, **850**, L34
- Becker A., 2015, HOTPANTS: High Order Transform of PSF ANd Template Subtraction (ascl:1504.004)
- Bellm E. C., et al., 2019, *PASP*, **131**, 068003
- Berger E., 2014, *Ann. Rev. Astron. Astrophys.*, **52**, 43
- Berger E., Fong W., Chornock R., 2013, *ApJ*, **774**, L23
- Bertin E., 2006, Automatic Astrometric and Photometric Calibration with SCAMP. p. 112
- Bertin E., 2011a, in Evans I. N., Accomazzi A., Mink D. J., Rots A. H., eds, *Astronomical Society of the Pacific Conference Series Vol. 442, Astronomical Data Analysis Software and Systems XX*. p. 435
- Bertin E., 2011b, Automated Morphometry with SExtractor and PSFEx. p. 435
- Bertin E., Arnouts S., 1996, *A&AS*, **117**, 393
- Bertin E., Mellier Y., Radovich M., Missonnier G., Didelon P., Morin B., 2002, in Bohlender D. A., Durand D., Handley T. H., eds, *Astronomical Society of the Pacific Conference Series Vol. 281, Astronomical Data Analysis Software and Systems XI*. p. 228
- Bloemen S., Groot P., Nelemans G., Klein-Wolt M., 2015, in Rucinski S. M., Torres G., Zejda M., eds, *Astronomical Society of the Pacific Conference Series Vol. 496, Living Together: Planets, Host Stars and Binaries*. p. 254
- Boch T., Fernique P., Bonnarel F., Chaitra C., Bot C., Pineau F. X., Baumann M., Michel L., 2020, in Pizzo R., Deul E. R., Mol J. D., de Plaa J., Verkouter H., eds, *Astronomical Society of the Pacific Conference Series Vol. 527, Astronomical Society of the Pacific Conference Series*. p. 121
- Bradley L., et al., 2021, *astropy/photutils*: 1.1.0, doi:10.5281/zenodo.4624996
- Brennan S. J., Fraser M., 2022, arXiv e-prints, p. arXiv:2201.02635
- Bulla M., 2019, *MNRAS*, **489**, 5037
- Chornock R., et al., 2017, *ApJ*, **848**, L19
- Coughlin M. W., et al., 2018, *Monthly Notices of the Royal Astronomical Society*, **480**, 3871
- Coughlin M. W., Dietrich T., Margalit B., Metzger B. D., 2019, *Monthly Notices of the Royal Astronomical Society: Letters*, **489**, L91
- Coughlin M. W., et al., 2020a, *Phys. Rev. Research*, **2**, 022006
- Coughlin M. W., et al., 2020b, *Nature Communications*, **11**, 4129
- Coughlin M. W., et al., 2020c, *MNRAS*, **492**, 863
- Coughlin M. W., et al., 2020d, *Monthly Notices of the Royal Astronomical Society*, **497**, 1181–1196
- Coulter D. A., et al., 2017, *Science*, **358**, 1556
- Cowperthwaite P. S., et al., 2017, *ApJ*, **848**, L17
- Cowperthwaite P. S., Villar V. A., Scolnic D. M., Berger E., 2019, *The Astrophysical Journal*, **874**, 88
- Dekany R., et al., 2020, *PASP*, **132**, 038001
- Dietrich T., Coughlin M. W., Pang P. T. H., Bulla M., Heinzl J., Issa L., Tews I., Antier S., 2020, *Science*, **370**, 1450
- Ducoin J.-G., Corre D., Leroy N., LeFloch E., 2020, *Monthly Notices of the Royal Astronomical Society*, **492**, 4768
- Duverne P. A., et al., 2022, MUPHOTEN : a MULTi-band PHOTometry Tool for TELEscope Network (arXiv:2201.07565)
- Flaugher B., et al., 2015, *AJ*, **150**, 150
- Ginsburg A., et al., 2019, *AJ*, **157**, 98
- Goldstein A., et al., 2017, *The Astrophysical Journal*, **848**, L14
- Gompertz B. P., et al., 2020, *Monthly Notices of the Royal Astronomical Society*, **497**, 726–738
- Graham M. J., et al., 2019, *PASP*, **131**, 078001
- Haggard D., Nynka M., Ruan J. J., Kalogera V., Cenko S. B., Evans P., Kennea J. A., 2017, *ApJ*, **848**, L25
- Hallinan G., et al., 2017, *Science*, **358**, 1579
- Ho A. Y. Q., et al., 2022, arXiv e-prints, p. arXiv:2201.12366
- Hotokezaka K., Nakar E., Gottlieb O., Nissanke S., Masuda K., Hallinan G., Mooley K. P., Deller A. T., 2019, *Nature Astronomy*, **3**, 940
- Hu L., et al., 2017, *Science Bulletin*, **62**, 1433
- Ivezić Ž., et al., 2019, *ApJ*, **873**, 111
- Karpov S., 2021, STDPipe: Simple Transient Detection Pipeline (ascl:2112.006)
- Kasen D., Metzger B., Barnes J., Quataert E., Ramirez-Ruiz E., 2017, *Nature*, **551**, 80–84
- Kasliwal M. M., et al., 2020, *The Astrophysical Journal*, **905**, 145
- Kostov A., Bonev T., 2018, *Bulgarian Astronomical Journal*, **28**, 3
- Lang D., Hogg D. W., Mierle K., Blanton M., Roweis S., 2010, *AJ*, **139**, 1782
- Levan A., et al., 2005, *ApJ*, **624**, 880
- Margalit B., Metzger B. D., 2017, *ApJ*, **850**, L19
- Margutti R., et al., 2018, Target of Opportunity Observations of Gravitational Wave Events with LSST (arXiv:1812.04051)
- Masci F. J., et al., 2019, *PASP*, **131**, 018003
- McCully C., Tewes M., 2019, Astro-SCRAPPY: Speedy Cosmic Ray Annihilation Package in Python (ascl:1907.032)
- Morgan J. S., Kaiser N., Moreau V., Anderson D., Burgett W., 2012, in Stepp L. M., Gilmozzi R., Hall H. J., eds, *Society of Photo-Optical Instrumentation Engineers (SPIE) Conference Series Vol. 8444, Ground-based and Airborne Telescopes IV*. p. 84440H (arXiv:1207.2513), doi:10.1117/12.926646
- Möller A., et al., 2020, *Monthly Notices of the Royal Astronomical Society*, **501**, 3272
- Patterson M. T., et al., 2019, *PASP*, **131**, 018001
- Perley D. A., et al., 2019, *MNRAS*, **484**, 1031
- Petrov P., et al., 2022, *ApJ*, **924**, 54
- Piro A. L., Haynie A., Yao Y., 2021, *The Astrophysical Journal*, **909**, 209
- Savchenko V., et al., 2017, *The Astrophysical Journal*, **848**, L15
- Tanvir N. R., Levan A. J., Fruchter A. S., Hjorth J., Hounsell R. A., Wiersema K., Tunnicliffe R. L., 2013, *Nature*, **500**, 547
- Tonry J. L., et al., 2018, *PASP*, **130**, 064505
- Troja E., et al., 2018, *Monthly Notices of the Royal Astronomical Society*,
- Waters C. Z., et al., 2020, *ApJS*, **251**, 4
- van Dokkum P. G., 2001, *PASP*, **113**, 1420

APPENDIX A: OBSERVATIONS FROM THE GRANDMA PROGRAM

APPENDIX B: LINEAR FITTING REGRESSION

The maximum likelihood approach is used to constrain the nature of the rapidly evolving transient phenomena. Maximum likelihood estimation (MLE) is a general method for estimating the best-fitting parameters (θ) of a statistical model, under the assumption that the true distribution of these parameters is known. Fitting any mathematical form of the model, these estimates maximize the probability of the observed values across a series of observations of a random variable. We use the concept of a sufficient statistic (S_{tt} , S_y) which contains all the information from the data that is needed to find the best-fitting θ parameters. Our maximum likelihood estimation function is defined as follows:

Table A1. Upper limits - Summary of the GRANDMA observations of some KN-MANGROVE alerts. δt is the delay between the beginning of the observation and the public detection discovery. In this table, only **upper limits** useful to confirm the nature of the source as moving objects are reported. Magnitudes are given in the AB system and not correct for Galactic extinction, upper limits are given at 5σ confidence.

Source	Obs date	Time	δt (days)	filter	Detec./Upper (mag)	Telescope/Observer	Reduction pipeline
ZTF21abdwdwo	2021-06-04	04:27:26	0.0	r'	18.8 ± 0.1	ZTF	ZTF
ZTF21abdwdwo	2021-06-05	00:00:00	0.8	Clear	> 20.7	T40-A77DAU	Muphoten
ZTF21abdwdwo	2021-06-07	21:41:04	3.7	B	> 21.4	T-CAT	Muphoten
ZTF21abxkven	2021-09-03	08:28:07	0.0	r'	18.4 ± 0.1	ZTF	ZTF
ZTF21abxkven	2021-09-03	22:13:14	0.5	B	> 19.0	Abastumani-T70	Muphoten
ZTF21abxkven	2021-09-03	22:14:28	0.5	R_C	> 18.8	Abastumani-T70	Muphoten
ZTF21abxkven	2021-09-03	22:35:46	0.5	L	> 18.2	K26	Muphoten
ZTF21abxkven	2021-09-04	02:42:20	0.7	L	> 20.6	T-ST SOPHIE	Muphoten
ZTF21abxkven	2021-09-04	13:07:55	1.6	Clear	> 20.6	T40-A77DAU	Muphoten
ZTF21abxlpdl	2021-09-03	08:59:16	0.0	r'	19.3 ± 0.1	ZTF	ZTF
ZTF21abxlpdl	2021-09-03	20:56:08	0.5	B	> 19.1	Abastumani-T70	Muphoten
ZTF21abxlpdl	2021-09-03	20:57:22	0.5	R_C	> 19.1	Abastumani-T70	Muphoten
ZTF21abxlpdl	2021-09-04	23:32:00	1.6	Clear	> 20.7	T40-A77DAU	Muphoten
ZTF21abyplur	2021-09-06	09:12:27	0.0	r'	17.5 ± 0.1	ZTF	ZTF
ZTF21abyplur	2021-09-15	21:17:03	9.5	g'	> 18.3	Tibet-50	Muphoten

$$\begin{aligned}
 L(\theta) &= L(a, b) \\
 &= \log P(y|a, b, H) \\
 &= -\frac{1}{2} \sum_i \log 2\pi\sigma_i^2 - \frac{1}{2} \sum_i \frac{(y_i - at_i - b)^2}{\sigma_i^2}
 \end{aligned}$$

Where, σ_i is the error of the measure of the magnitude y_i at the date t_i .

The sufficient statistics, S_{tt} and S_y , are zeros of the partial first derivatives of log maximum likelihood $L(\theta)$.

$$\frac{\partial \log L}{\partial \theta} = 0$$

This gives us :

$$\begin{cases}
 S_{tt} = a \sum_i \frac{t_i^2}{\sigma_i^2} + b \sum_i \frac{t_i}{\sigma_i^2} = \sum_i \frac{t_i y_i}{\sigma_i^2} \\
 S_y = a \sum_i \frac{t_i}{\sigma_i^2} + b \sum_i \frac{1}{\sigma_i^2} = \sum_i \frac{y_i}{\sigma_i^2}
 \end{cases}$$

The best-fitting estimators (a, b) are given following the resolution of these linear equations above. And our linear regression is defined by $Y_i = at_i + b$. The parameter a is our light linear evolution rate. We define a **slow transient**, a transient whose decay rate is either negative (the brightness rises) or below 0.3 mag/day in a given filter.

APPENDIX C: AFFILIATIONS

¹E. Kharadze Georgian National Astrophysical Observatory, Mt.Kanobili, Abastumani, 0301, Adigeni, Georgia; Iliia State University, Kakutsa Cholokashvili ave 3/5, Tbilisi 0162, Georgia

²Samskhe-Javakheti State University, Rustaveli Str. 113, Akhaltsikhe, 0080, Georgia

³American University of Sharjah, Physics Department, PO Box 26666, Sharjah, UAE

⁴Artemis, Observatoire de la Côte d'Azur, Université Côte d'Azur, Boulevard de l'Observatoire, 06304 Nice, France

⁵GRAPPA, Anton Pannekoek Institute for Astronomy and

Institute of High-Energy Physics, University of Amsterdam, Science Park 904,1098 XH Amsterdam, The Netherlands

⁶Université de Paris, CNRS, Astroparticule et Cosmologie, F-75013 Paris, France

⁷Astronomical Observatory Taras Shevshenko National University of Kyiv, Observatorna str. 3, Kyiv, 04053, Ukraine

⁸University of Iceland, Sæmundargata 2, 102 Reykjavík, Iceland

⁹Aix Marseille Univ, CNRS, CNES, LAM, IPHu, Marseille, France

¹⁰Société Astronomique de Lyon, 9 Avenue Charles André, Saint Genis Laval, France

¹¹ICAMER Observatory of NAS of Ukraine 27 Acad. Zabolotnoho Str., Kyiv, 03143, Ukraine

¹²Instituto de Astrofísica de Andalucía (IAA-CSIC), Glorieta de la Astronomía s/n, 18008 Granada, Spain

¹³Université Grenoble-Alpes, Université Savoie Mont Blanc, CNRS/IN2P3 Laboratoire d'Annecy-le-Vieux de Physique des particules, France

¹⁴Observatoire de Dauban, 04 Banon - France

¹⁵Groupe Astronomique de Querqueville, 61, rue Roger Glinel, 50460, Cherbourg en cotentin, France

¹⁶Vereniging Voor Sterrenkunde, Balen-Neetlaan 18A, B-2400, Mol, Belgium

¹⁷Zeeweg 96, B-8200 Brugge, Belgium

¹⁸Ulugh Beg Astronomical Institute, Uzbekistan Academy of Sciences, Astronomy str. 33, Tashkent 100052, Uzbekistan

¹⁹MP-G2A, Midi Pyrénées, Groud Astrophysic Addict, 81570, Cuq, France

²⁰El Center for Backyard Astrophysics, Spain

²¹School of Physics and Astronomy, University of Minnesota, Minneapolis, Minnesota 55455, USA

²²Institute for Physics and Astronomy, University of Potsdam, D-14476 Potsdam, Germany

²³Max Planck Institute for Gravitational Physics (Albert Einstein Institute), Am Mühlenberg 1, D-14476

²⁴OHP, Observatoire de Haute-Provence, CNRS, Aix Marseille University, Institut Pythéas, St Michel l'Observatoire, France

Table A2. Detections - Summary of the GRANDMA observations of ZTF-Fink candidates. δt is the delay between the beginning of the observation and the public detection discovery. In this table, only detection magnitudes of each observational epoch are reported. Magnitudes are given in the AB system and not correct for Galactic extinction.

Source	Obs date	Time	δt (days)	filter	Detec. mag (STDpipe)	mag. Muphoten (or ZTF)	Telescope/Observer
ZTF21abbzjeq	2021-05-20	09:28:49	0.0	g'	-	19.7 ± 0.2	ZTF
ZTF21abbzjeq	2021-05-27	07:35:33	6.9	g'	-	17.5 ± 0.1	ZTF
ZTF21abbzjeq	2021-05-27	09:12:08	7.0	r'	-	17.7 ± 0.1	ZTF
ZTF21abbzjeq	2021-05-28	22:14:18	8.5	V	17.5 ± 0.1	17.5 ± 0.1	T-BRO
ZTF21abbzjeq	2021-05-28	22:29:27	8.5	R	17.4 ± 0.1	17.4 ± 0.1	T-BRO
ZTF21abbzjeq	2021-05-28	22:49:12	8.6	B	17.4 ± 0.1	17.4 ± 0.1	T-BRO
ZTF21abbzjeq	2021-05-28	23:10:23	8.6	I	17.5 ± 0.1	17.4 ± 0.1	T-BRO
ZTF21abbzjeq	2021-05-29	06:44:06	8.9	g'	-	17.3 ± 0.1	ZTF
ZTF21abbzjeq	2021-05-31	08:25:51	11.0	r'	-	17.3 ± 0.1	ZTF
ZTF21abbzjeq	2021-05-31	22:53:44	11.6	R	17.2 ± 0.1	17.2 ± 0.1	Omegon203
ZTF21abbzjeq	2021-06-02	07:10:42	12.9	g'	-	17.1 ± 0.1	ZTF
ZTF21abbzjeq	2021-08-01	06:17:15	72.9	g'	-	20.1 ± 0.1	ZTF
ZTF21abbzjeq	2021-08-03	00:44:35	74.6	R	19.1 ± 0.1	19.0 ± 0.1	VIRT
ZTF21abbzjeq	2021-08-03	17:58:53	75.3	B	20.1 ± 0.1	20.3 ± 0.1	Abastumani/T70
ZTF21abbzjeq	2021-08-03	18:01:07	75.4	R_C	18.9 ± 0.1	18.9 ± 0.1	Abastumani/T70
ZTF21abbzjeq	2021-08-04	04:40:50	75.8	R	19.3 ± 0.2	18.9 ± 0.2	TRT-SRO
ZTF21abbzjeq	2021-08-04	06:23:46	75.9	I	19.2 ± 0.2	19.4 ± 0.2	TRT-SRO
ZTF21abbzjeq	2021-08-08	04:29:20	79.8	r'	-	19.6 ± 0.2	ZTF
ZTF21abbzjeq	2021-08-08	05:40:55	79.8	g'	-	20.2 ± 0.3	ZTF
ZTF21abfaohe	2021-06-09	05:14:26	0.0	g'	-	19.4 ± 0.2	ZTF
ZTF21abfaohe	2021-06-22	04:32:33	13.0	r'	-	14.4 ± 0.2	ZTF
ZTF21abfaohe	2021-06-22	07:02:41	13.1	g'	-	14.3 ± 0.2	ZTF
ZTF21abfaohe	2021-06-25	20:23:39	16.6	r'	14.2 ± 0.1	14.2 ± 0.2	Iris
ZTF21abfaohe	2021-06-25	21:02:47	16.7	g'	14.1 ± 0.1	14.1 ± 0.2	Iris
ZTF21abfaohe	2021-06-25	21:23:27	16.7	G	14.2 ± 0.1	-	PDAObs
ZTF21abfaohe	2021-06-25	22:01:28	16.7	B	14.2 ± 0.1	14.5 ± 0.1	T-CAT
ZTF21abfaohe	2021-06-25	22:01:28	16.7	G	14.2 ± 0.1	14.4 ± 0.1	T-CAT
ZTF21abfaohe	2021-06-25	22:01:28	16.7	R	14.1 ± 0.1	13.9 ± 0.1	T-CAT
ZTF21abfaohe	2021-06-25	22:10:50	16.7	R	14.2 ± 0.1	-	PDAObs
ZTF21abfaohe	2021-06-25	22:58:41	16.8	G	14.2 ± 0.1	-	PDAObs
ZTF21abfaohe	2021-06-26	00:00:00	16.8	Clear	14.1 ± 0.1	13.5 ± 0.1	T40-A77DAU
ZTF21abfaohe	2021-06-26	05:07:59	17.0	g'	-	14.1 ± 0.1	ZTF
ZTF21abfaohe	2021-06-26	06:32:45	17.1	r'	-	14.3 ± 0.1	ZTF
ZTF21abfaohe	2021-06-26	20:18:11	17.6	Clear	14.1 ± 0.1	-	MSXD-A77
ZTF21abfaohe	2021-06-26	20:26:08	17.7	R	14.2 ± 0.1	-	MSXD-A77
ZTF21abfaohe	2021-06-27	21:42:45	18.7	Clear	14.1 ± 0.1	13.6 ± 0.1	T40-A77DAU
ZTF21abfaohe	2021-06-28	05:04:28	19.0	r'	-	14.3 ± 0.1	ZTF
ZTF21abfaohe	2021-06-28	07:02:23	19.1	g'	-	14.2 ± 0.1	ZTF
ZTF21abfaohe	2021-06-28	09:11:07	19.2	r'	14.2 ± 0.1	14.3 ± 0.1	iTel-17
ZTF21abfaohe	2021-06-28	09:21:10	19.2	g'	14.1 ± 0.1	14.2 ± 0.1	iTel-17
ZTF21abfaohe	2021-06-30	05:35:16	21.0	g'	-	14.2 ± 0.1	ZTF
ZTF21abfaohe	2021-07-01	21:32:09	22.7	Clear	14.2 ± 0.1	13.7 ± 0.1	T40-A77DAU
ZTF21abfaohe	2021-07-02	05:34:58	23.0	g'	-	14.2 ± 0.1	ZTF
ZTF21abfaohe	2021-07-04	07:19:38	25.1	Clear	14.3 ± 0.1	13.9 ± 0.3	Beverly-Begg
ZTF21abfaohe	2021-07-04	23:02:45	25.8	B	14.5 ± 0.1	14.9 ± 0.1	T-CAT
ZTF21abfaohe	2021-07-04	23:02:45	25.8	G	14.4 ± 0.1	14.7 ± 0.1	T-CAT
ZTF21abfaohe	2021-07-04	23:02:45	25.8	R	14.4 ± 0.1	14.2 ± 0.1	T-CAT
ZTF21abfaohe	2021-07-05	04:34:55	26.0	r'	-	14.5 ± 0.1	ZTF
ZTF21abfaohe	2021-07-05	06:05:02	26.1	g'	-	14.4 ± 0.1	ZTF
ZTF21abfaohe	2021-07-07	05:32:50	27.0	r'	-	14.7 ± 0.1	ZTF
ZTF21abfaohe	2021-07-08	20:34:29	29.7	Clear	14.7 ± 0.1	14.3 ± 0.1	ZnithObs
ZTF21abfaohe	2021-07-09	05:29:28	30.0	r'	-	14.9 ± 0.1	ZTF
ZTF21abfaohe	2021-07-28	04:38:47	49.0	g'	-	16.5 ± 0.1	ZTF
ZTF21abfaohe	2021-07-31	00:46:46	52.8	R_C	15.5 ± 0.1	-	FRAM-Auger
ZTF21abfaohe	2021-08-01	04:16:28	53.0	r'	-	15.8 ± 0.1	ZTF
ZTF21abfaohe	2021-08-03	17:21:26	55.5	B	17.1 ± 0.1	17.1 ± 0.1	Abastumani/T70
ZTF21abfaohe	2021-08-03	17:22:40	55.5	R_C	15.9 ± 0.1	15.9 ± 0.1	Abastumani/T70
ZTF21abfmbix	2021-06-11	05:14:49	0.0	g'	-	18.1 ± 0.10	ZTF
ZTF21abfmbix	2021-06-11	06:05:58	0.1	r'	-	17.8 ± 0.10	ZTF
ZTF21abfmbix	2021-06-11	21:09:01	0.7	L	17.4 ± 0.1	16.4 ± 0.2	Uranoscope
ZTF21abfmbix	2021-06-11	21:21:33	0.7	R	17.4 ± 0.1	17.2 ± 0.2	MSXD-A77
ZTF21abfmbix	2021-06-11	21:41:37	0.7	L	17.0 ± 0.1	16.8 ± 0.2	Teams
ZTF21abfmbix	2021-06-11	21:54:07	0.7	R	17.4 ± 0.1	17.2 ± 0.1	T-CAT

Table A2. Continued.

Source	Obs date	Time	δt (days)	filter	Detec. mag (STDpipe)	Muphoten (or ZTF)	Telescope/Observer
ZTF21abfmbix	2021-06-11	21:54:07	0.7	<i>B</i>	17.8 ± 0.1	18.1 ± 0.1	T-CAT
ZTF21abfmbix	2021-06-11	21:54:07	0.7	<i>G</i>	17.5 ± 0.1	17.5 ± 0.1	T-CAT
ZTF21abfmbix	2021-06-11	22:20:06	0.7	<i>R</i>	17.4 ± 0.1	17.4 ± 0.2	Vallieres
ZTF21abfmbix	2021-06-12	21:20:54	1.7	Clear	17.1 ± 0.2	16.9 ± 0.2	T-GRA
ZTF21abfmbix	2021-06-12	21:42:53	1.7	<i>R</i>	17.0 ± 0.1	16.6 ± 0.1	T-CAT
ZTF21abfmbix	2021-06-12	21:42:53	1.7	<i>B</i>	17.2 ± 0.1	17.6 ± 0.1	T-CAT
ZTF21abfmbix	2021-06-12	21:42:53	1.7	<i>G</i>	17.1 ± 0.1	17.4 ± 0.1	T-CAT
ZTF21abfmbix	2021-06-12	21:46:29	1.7	<i>L</i>	17.0 ± 0.1	16.8 ± 0.2	N250-ROU
ZTF21abfmbix	2021-06-13	02:56:45	1.9	Clear	16.9 ± 0.1	16.5 ± 0.5	RIT
ZTF21abfmbix	2021-06-13	04:25:03	2.0	<i>G</i>	17.0 ± 0.1	17.0 ± 0.1	C11FREE
ZTF21abfmbix	2021-06-13	04:25:03	2.0	<i>R</i>	16.9 ± 0.1	16.9 ± 0.2	C11FREE
ZTF21abfmbix	2021-06-13	04:38:39	2.0	<i>g'</i>	-	17.1 ± 0.1	ZTF
ZTF21abfmbix	2021-06-13	05:43:19	2.0	<i>V</i>	17.0 ± 0.1	17.0 ± 0.1	iTel-24
ZTF21abfmbix	2021-06-13	05:51:15	2.0	<i>I</i>	17.0 ± 0.2	17.1 ± 0.1	iTel-24
ZTF21abfmbix	2021-06-13	05:59:57	2.0	<i>r'</i>	-	16.9 ± 0.1	ZTF
ZTF21abfmbix	2021-06-13	21:53:06	2.7	<i>R</i>	16.6 ± 0.1	16.4 ± 0.1	T-CAT
ZTF21abfmbix	2021-06-13	21:53:06	2.7	<i>B</i>	16.9 ± 0.1	17.2 ± 0.1	T-CAT
ZTF21abfmbix	2021-06-13	21:53:06	2.7	<i>G</i>	16.8 ± 0.1	16.9 ± 0.1	T-CAT
ZTF21abfmbix	2021-06-13	22:00:44	2.7	<i>R</i>	16.7 ± 0.1	16.5 ± 0.1	Omegon23
ZTF21abfmbix	2021-07-01	04:29:46	20.0	<i>r'</i>	-	15.5 ± 0.1	ZTF
ZTF21abfmbix	2021-07-01	05:59:37	20.0	<i>g'</i>	-	16.2 ± 0.1	ZTF
ZTF21abfmbix	2021-07-04	22:35:05	23.7	<i>R</i>	15.7 ± 0.1	15.5 ± 0.1	T-CAT
ZTF21abfmbix	2021-07-04	22:35:05	23.7	<i>B</i>	16.7 ± 0.1	17.1 ± 0.1	T-CAT
ZTF21abfmbix	2021-07-04	22:35:05	23.7	<i>G</i>	16.1 ± 0.1	16.2 ± 0.1	T-CAT
ZTF21abfmbix	2021-07-10	21:21:06	29.7	Clear	16.2 ± 0.1	15.2 ± 0.1	T40-A77DAU
ZTF21ablssud	2021-07-14	07:06:24	0.0	<i>r'</i>	-	16.4 ± 0.1	ZTF
ZTF21ablssud	2021-07-14	08:00:27	0.0	<i>g'</i>	-	16.4 ± 0.1	ZTF
ZTF21ablssud	2021-07-16	06:25:45	2.0	<i>r'</i>	-	16.7 ± 0.1	ZTF
ZTF21ablssud	2021-07-16	07:34:52	2.0	<i>g'</i>	-	16.9 ± 0.1	ZTF
ZTF21ablssud	2021-07-16	21:11:45	2.6	<i>G</i>	17.0 ± 0.1	16.9 ± 0.1	PDAObs
ZTF21ablssud	2021-07-16	21:34:49	2.6	<i>V</i>	17.0 ± 0.1	17.0 ± 0.1	Gallinero
ZTF21ablssud	2021-07-16	21:39:48	2.6	<i>G</i>	16.8 ± 0.1	17.4 ± 0.1	T-CAT
ZTF21ablssud	2021-07-16	21:39:48	2.6	<i>B</i>	17.1 ± 0.1	17.7 ± 0.1	T-CAT
ZTF21ablssud	2021-07-16	21:39:48	2.6	<i>R</i>	16.7 ± 0.1	16.6 ± 0.1	T-CAT
ZTF21ablssud	2021-07-16	21:42:04	2.6	<i>R</i>	16.8 ± 0.1	16.5 ± 0.1	PDAObs
ZTF21ablssud	2021-07-16	22:12:09	2.6	<i>I</i>	16.5 ± 0.1	16.6 ± 0.1	PDAObs
ZTF21ablssud	2021-07-16	22:18:17	2.6	<i>L</i>	16.7 ± 0.1	16.1 ± 0.1	Uranoscope
ZTF21ablssud	2021-07-16	22:24:00	2.6	Clear	16.7 ± 0.1	16.0 ± 0.1	MSXD-A77
ZTF21ablssud	2021-07-17	21:21:24	3.6	Clear	16.9 ± 0.1	16.4 ± 0.1	T40-A77DAU
ZTF21ablssud	2021-07-17	21:34:01	3.6	<i>V</i>	16.9 ± 0.1	16.8 ± 0.1	Omegon203
ZTF21ablssud	2021-07-17	21:35:18	3.6	<i>V</i>	17.2 ± 0.1	17.2 ± 0.1	Gallinero
ZTF21ablssud	2021-07-17	21:48:52	3.6	<i>R</i>	17.0 ± 0.1	16.8 ± 0.2	N250-ROU
ZTF21ablssud	2021-07-17	21:59:42	3.6	<i>R</i>	16.9 ± 0.1	16.7 ± 0.2	Montarrenti
ZTF21ablssud	2021-07-17	22:01:39	3.6	<i>B</i>	17.4 ± 0.1	17.6 ± 0.2	N250-ROU
ZTF21ablssud	2021-07-17	22:15:59	3.6	<i>G</i>	17.1 ± 0.1	17.3 ± 0.2	N250-ROU
ZTF21ablssud	2021-07-17	23:16:15	3.7	<i>R</i>	17.0 ± 0.1	16.9 ± 0.2	N250-ROU
ZTF21ablssud	2021-07-17	23:22:48	3.7	<i>B</i>	17.3 ± 0.1	17.6 ± 0.2	N250-ROU
ZTF21ablssud	2021-07-17	23:36:58	3.7	<i>B</i>	17.4 ± 0.1	17.5 ± 0.2	Montarrenti
ZTF21ablssud	2021-07-17	23:36:58	3.7	<i>R</i>	16.9 ± 0.1	17.0 ± 0.2	Montarrenti
ZTF21ablssud	2021-07-18	01:50:55	3.8	<i>B</i>	17.6 ± 0.2	17.6 ± 0.1	T-BRO
ZTF21ablssud	2021-07-18	02:03:09	3.8	<i>I</i>	16.7 ± 0.1	16.6 ± 0.1	T-BRO
ZTF21ablssud	2021-07-18	04:37:08	3.9	<i>R</i>	17.1 ± 0.1	16.8 ± 0.2	C11FREE
ZTF21ablssud	2021-07-18	04:37:08	3.9	<i>G</i>	17.5 ± 0.1	17.4 ± 0.1	C11FREE
ZTF21ablssud	2021-07-18	21:09:46	4.6	<i>g'</i>	17.2 ± 0.1	17.1 ± 0.1	PDAObs
ZTF21ablssud	2021-07-18	21:23:05	4.6	<i>R</i>	16.8 ± 0.1	17.0 ± 0.3	Vallieres
ZTF21ablssud	2021-07-18	21:29:49	4.6	Clear	16.9 ± 0.1	16.4 ± 0.1	T40-A77DAU
ZTF21ablssud	2021-07-18	21:40:09	4.6	<i>G</i>	17.1 ± 0.1	17.7 ± 0.1	T-CAT
ZTF21ablssud	2021-07-18	21:40:09	4.6	<i>R</i>	17.0 ± 0.1	16.8 ± 0.1	T-CAT
ZTF21ablssud	2021-07-18	21:40:09	4.6	<i>B</i>	17.4 ± 0.1	18.0 ± 0.1	T-CAT
ZTF21ablssud	2021-07-18	21:55:21	4.6	<i>r'</i>	17.1 ± 0.1	17.1 ± 0.1	PDAObs
ZTF21ablssud	2021-07-18	22:41:05	4.6	<i>i</i>	16.8 ± 0.1	16.9 ± 0.1	PDAObs
ZTF21ablssud	2021-07-19	01:45:49	4.8	<i>B</i>	17.6 ± 0.1	17.6 ± 0.1	T-BRO
ZTF21ablssud	2021-07-19	01:54:56	4.8	<i>V</i>	17.2 ± 0.1	17.3 ± 0.1	T-BRO
ZTF21ablssud	2021-07-19	02:04:03	4.8	<i>R</i>	17.0 ± 0.1	16.8 ± 0.1	T-BRO
ZTF21ablssud	2021-07-19	02:13:08	4.8	<i>I</i>	16.9 ± 0.1	16.6 ± 0.1	T-BRO

Table A2. Continued.

Source	Obs date	Time	δt (days)	filter	Detec. mag (STDpipe)	Muphoten (or ZTF)	Telescope/Observer
ZTF21ablssud	2021-07-19	07:06:07	5.0	r'	-	17.2 ± 0.1	ZTF
ZTF21ablssud	2021-07-19	21:02:35	5.6	<i>Clear</i>	17.2 ± 0.1	16.6 ± 0.1	T40-A77DAU
ZTF21ablssud	2021-07-19	21:23:50	5.6	R	17.1 ± 0.1	17.0 ± 0.2	Montarrenti
ZTF21ablssud	2021-07-19	22:12:46	5.6	L	17.3 ± 0.1	16.4 ± 0.1	K26
ZTF21ablssud	2021-07-19	22:19:51	5.6	R	17.2 ± 0.1	17.0 ± 0.1	T-CAT
ZTF21ablssud	2021-07-19	22:19:51	5.6	B	17.6 ± 0.1	18.2 ± 0.1	T-CAT
ZTF21ablssud	2021-07-19	22:19:51	5.6	G	17.3 ± 0.1	17.9 ± 0.1	T-CAT
ZTF21ablssud	2021-07-19	23:06:29	5.7	R	17.2 ± 0.1	17.2 ± 0.3	Montarrenti
ZTF21ablssud	2021-07-19	23:07:38	5.7	B	17.8 ± 0.1	18.0 ± 0.3	Montarrenti
ZTF21ablssud	2021-07-20	20:15:05	6.5	<i>Clear</i>	17.0 ± 0.1	16.7 ± 0.1	ZnithObs
ZTF21ablssud	2021-07-20	20:45:31	6.6	<i>Clear</i>	17.3 ± 0.1	16.9 ± 0.1	ZnithObs
ZTF21ablssud	2021-07-20	21:08:33	6.6	R	17.2 ± 0.1	17.3 ± 0.2	Montarrenti
ZTF21ablssud	2021-07-20	21:29:33	6.6	<i>Clear</i>	16.9 ± 0.1	16.7 ± 0.1	T40-A77DAU
ZTF21ablssud	2021-07-20	21:38:00	6.6	L	17.5 ± 0.1	16.5 ± 0.1	K26
ZTF21ablssud	2021-07-20	22:48:24	6.7	R	17.3 ± 0.1	17.6 ± 0.2	Montarrenti
ZTF21ablssud	2021-07-20	21:41:22	8.6	<i>Clear</i>	17.5 ± 0.1	17.1 ± 0.1	T40-A77DAU
ZTF21ablssud	2021-07-23	00:39:53	8.7	V	17.7 ± 0.1	17.6 ± 0.1	T-BRO
ZTF21ablssud	2021-07-23	00:49:00	8.7	R	17.4 ± 0.1	17.3 ± 0.1	T-BRO
ZTF21ablssud	2021-07-23	00:58:07	8.7	I	17.2 ± 0.2	17.2 ± 0.1	T-BRO
ZTF21ablssud	2021-07-23	01:14:57	8.8	<i>Clear</i>	17.5 ± 0.1	17.2 ± 0.1	T-BRO
ZTF21ablssud	2021-07-24	07:16:06	10.0	r'	-	17.8 ± 0.1	ZTF
ZTF21ablssud	2021-07-24	08:39:27	10.1	g'	-	18.0 ± 0.1	ZTF
ZTF21ablssud	2021-07-27	21:51:12	13.6	R	17.8 ± 0.1	17.5 ± 0.3	Montarrenti
ZTF21ablssud	2021-07-28	07:12:16	14.0	r'	-	18.1 ± 0.1	ZTF
ZTF21ablssud	2021-07-28	08:05:58	14.0	g'	-	18.2 ± 0.1	ZTF
ZTF21ablssud	2021-07-29	21:16:28	15.6	B	18.8 ± 0.1	18.8 ± 0.2	Montarrenti
ZTF21ablssud	2021-07-29	21:17:37	15.6	R	18.1 ± 0.2	18.0 ± 0.1	Montarrenti
ZTF21ablssud	2021-07-30	07:59:11	16.0	r'	-	18.2 ± 0.1	ZTF
ZTF21ablssud	2021-07-30	08:40:48	16.1	g'	-	18.6 ± 0.1	ZTF
ZTF21ablssud	2021-08-02	00:42:03	18.7	B	19.0 ± 0.1	19.0 ± 0.2	VIRT
ZTF21ablssud	2021-08-02	04:01:46	18.9	R	18.4 ± 0.1	18.0 ± 0.1	VIRT
ZTF21ablssud	2021-08-02	06:15:48	19.0	g'	-	18.9 ± 0.1	ZTF
ZTF21ablssud	2021-08-02	10:32:43	19.1	R	18.3 ± 0.1	18.2 ± 0.1	TRT-SRO
ZTF21ablssud	2021-08-04	05:38:52	20.9	r'	-	18.7 ± 0.1	ZTF
ZTF21ablssud	2021-08-04	07:12:07	21.0	g'	-	19.0 ± 0.1	ZTF
ZTF21ablssud	2021-08-05	04:53:24	21.9	I	18.3 ± 0.1	18.6 ± 0.2	TRT-SRO
ZTF21ablssud	2021-08-06	05:14:32	22.9	I	18.5 ± 0.1	18.6 ± 0.1	TRT-SRO
ZTF21ablssud	2021-08-09	05:59:45	25.9	r'	-	18.9 ± 0.1	ZTF
ZTF21ablssud	2021-08-09	22:48:05	26.7	I	18.4 ± 0.2	18.2 ± 0.1	UBAI/NT-60
ZTF21ablssud	2021-08-09	22:54:20	26.7	R	18.5 ± 0.2	18.5 ± 0.1	UBAI/NT-60
ZTF21ablssud	2021-08-10	21:42:37	27.6	I	18.8 ± 0.2	18.6 ± 0.1	UBAI/NT-60

²⁵IJCLab, Univ Paris-Saclay, CNRS/IN2P3, Orsay, France²⁶Institut d'Astrophysique de Paris, 98 bis boulevard Arago, 75014 Paris France²⁷Institute of Earth Systems, University of Malta, MSD 2080, Malta²⁸Znith Observatory, Naxxar, Malta²⁹APPAM, Montredon-Labessonnié, France³⁰University of the Virgin Islands, United States Virgin Islands 00802, USA³¹Volkssternwarte Paderborn, Im Schloßpark 13,33104 Paderborn, Germany³²Hidden Valley Observatory, E9891 810th Ave., Colfax, WI., USA³³LPC, Université Clermont Auvergne, CNES/IN2P3, F-63000, France³⁴Dunedin Astronomical Society (DAS), Royal Astronomical Society of New Zealand³⁵FZU - Institute of Physics of the Czech Academy of Sciences, Na Slovance 1999/2, CZ-182 21, Praha, Czech Republic³⁶Laboratoire de Physique et de Chimie de l'Environnement, Université Joseph KI-ZERBO, Ouagadougou, Burkina Faso³⁷IRAP, Université de Toulouse, CNRS, UPS, 14 Avenue Edouard Belin, F-31400 Toulouse, France³⁸Université Paul Sabatier Toulouse III, Université de Toulouse, 118 route de Narbonne, 31400 Toulouse, France³⁹Contern Observatory, L-5316 Contern, Luxembourg⁴⁰Beijing Planetarium, Beijing Academy of Science and Technology, Beijing, 100044, China⁴¹Montarrenti Observatory, S.S. 73 Ponente, I-53018, Sovicille, Siena, Italy⁴²OPERA Z97-, 33820 Saint Palais, France⁴³Observatory Uranoscope de l'Île de France, Allée Camille Flammarion 77220 Gretz-Armainvilliers, France⁴⁴Observatoire du "Crous des Gats", 31550 Cintegabelle, France⁴⁵Centre for Astrophysics and Supercomputing, Swinburne University of Technology, Mail Number H29, PO Box 218, 31122 Hawthorn, VIC, Australia⁴⁶OAR Telescope/NSF's NOIRLab, Avda Juan Cisternas

Table A2. Continued.

Source	Obs date	Time	δt (days)	filter	Detec. mag (STDpipe)	Muphoten (or ZTF)	Telescope/Observer
ZTF21abotose	2021-07-28	05:10:28	0.0	g'	-	18.7 ± 0.1	ZTF
ZTF21abotose	2021-07-30	04:41:20	2.0	r'	-	19.1 ± 0.1	ZTF
ZTF21abotose	2021-07-30	05:28:22	2.0	g'	-	19.3 ± 0.1	ZTF
ZTF21abotose	2021-07-30	20:05:42	2.6	R	18.7 ± 0.1	18.7 ± 0.1	Montarrenti
ZTF21abotose	2021-07-30	21:13:22	2.7	Clear	19.4 ± 0.2	18.8 ± 0.1	T40-A77DAU
ZTF21abotose	2021-07-30	04:39:44	4.0	r'	-	19.7 ± 0.2	ZTF
ZTF21abotose	2021-07-30	05:36:13	4.0	g'	-	19.8 ± 0.2	ZTF
ZTF21abotose	2021-08-01	20:50:06	4.7	Clear	19.2 ± 0.1	19.3 ± 0.1	MSXD-A77
ZTF21abotose	2021-08-08	06:06:33	6.1	g'	-	20.2 ± 0.2	ZTF
ZTF21abotose	2021-08-04	21:44:34	7.7	B	20.1 ± 0.1	20.2 ± 0.1	T-CAT
ZTF21abotose	2021-08-04	21:44:34	7.7	R	19.6 ± 0.1	19.5 ± 0.1	T-CAT
ZTF21abotose	2021-08-06	22:09:01	9.7	B	19.8 ± 0.1	19.9 ± 0.1	T-CAT
ZTF21abotose	2021-08-06	22:09:01	9.7	G	19.8 ± 0.1	20.3 ± 0.1	T-CAT
ZTF21abotose	2021-08-06	22:09:01	9.7	R	19.2 ± 0.1	19.3 ± 0.1	T-CAT
ZTF21abotose	2021-08-08	22:49:42	11.8	B	19.6 ± 0.1	19.7 ± 0.1	T-CAT
ZTF21abotose	2021-08-08	22:49:42	11.8	G	19.4 ± 0.1	19.9 ± 0.1	T-CAT
ZTF21abotose	2021-08-08	22:49:42	11.8	R	19.0 ± 0.1	19.0 ± 0.1	T-CAT
ZTF21abotose	2021-08-09	21:55:18	12.7	B	19.4 ± 0.1	19.5 ± 0.1	T-CAT
ZTF21abotose	2021-08-09	21:55:18	12.7	G	19.4 ± 0.1	19.5 ± 0.1	T-CAT
ZTF21abotose	2021-08-09	21:55:18	12.7	R	18.9 ± 0.1	19.0 ± 0.1	T-CAT
ZTF21abotose	2021-08-10	05:08:49	13.0	r'	-	19.0 ± 0.2	ZTF
ZTF21abotose	2021-08-10	05:39:08	13.0	g'	-	19.2 ± 0.2	ZTF
ZTF21abotose	2021-08-10	22:05:26	13.7	B	19.6 ± 0.1	19.6 ± 0.1	T-CAT
ZTF21abotose	2021-08-10	22:05:26	13.7	G	19.3 ± 0.1	19.4 ± 0.1	T-CAT
ZTF21abotose	2021-08-10	22:05:26	13.7	R	18.8 ± 0.1	18.7 ± 0.1	T-CAT
ZTF21abotose	2021-08-11	20:45:01	14.7	B	19.4 ± 0.1	19.3 ± 0.1	T-CAT
ZTF21abotose	2021-08-13	04:14:25	16.0	g'	-	19.2 ± 0.2	ZTF
ZTF21abotose	2021-08-13	21:50:45	16.7	G	18.8 ± 0.1	19.1 ± 0.1	T-CAT
ZTF21abotose	2021-08-13	21:50:45	16.7	R	18.7 ± 0.1	18.9 ± 0.1	T-CAT
ZTF21abotose	2021-08-15	04:09:00	18.0	r'	-	18.6 ± 0.1	ZTF
ZTF21abotose	2021-08-15	05:52:39	18.0	g'	-	19.0 ± 0.2	ZTF
ZTF21abotose	2021-08-15	05:52:39	31.1	r'	-	19.1 ± 0.2	ZTF
ZTF21abotose	2021-08-29	21:16:13	32.7	B	20.8 ± 0.1	20.9 ± 0.1	T-CAT
ZTF21abotose	2021-08-29	21:16:13	32.7	G	19.7 ± 0.1	20.5 ± 0.1	T-CAT
ZTF21abotose	2021-08-29	21:16:13	32.7	R	19.3 ± 0.1	19.3 ± 0.1	T-CAT
ZTF21abotose	2021-08-31	05:19:56	34.0	g'	-	20.1 ± 0.3	ZTF
ZTF21absvlrr	2021-08-12	09:52:43	0.0	g'	-	18.7 ± 0.20	ZTF
ZTF21absvlrr	2021-08-12	11:05:04	0.1	r'	-	18.6 ± 0.10	ZTF
ZTF21absvlrr	2021-08-13	09:23:51	1.0	r'	18.5 ± 0.1	18.5 ± 0.1	T-PDA
ZTF21absvlrr	2021-08-13	12:18:58	1.1	Clear	18.0 ± 0.1	17.4 ± 0.1	Beverly-Begg
ZTF21absvlrr	2021-08-14	02:01:14	1.7	B	18.0 ± 0.2	17.9 ± 0.1	Montarrenti
ZTF21absvlrr	2021-08-14	02:02:22	1.7	R	17.7 ± 0.1	17.5 ± 0.1	Montarrenti
ZTF21absvlrr	2021-08-14	10:02:31	2.0	g'	-	17.6 ± 0.1	ZTF
ZTF21absvlrr	2021-08-14	11:04:16	2.0	r'	-	17.7 ± 0.1	ZTF
ZTF21absvlrr	2021-08-15	03:13:25	2.7	Clear	17.3 ± 0.1	16.6 ± 0.1	T40-A77DAU
ZTF21absvlrr	2021-08-16	10:08:03	4.0	r'	-	17.0 ± 0.1	ZTF
ZTF21absvlrr	2021-08-17	12:50:20	4.1	V	16.7 ± 0.1	16.6 ± 0.1	TRT-SBO
ZTF21absvlrr	2021-08-17	11:03:01	5.1	r'	-	16.7 ± 0.1	ZTF
ZTF21absvlrr	2021-08-19	10:38:15	7.0	R	16.1 ± 0.1	16.2 ± 0.2	TRT-SBO
ZTF21absvlrr	2021-08-20	09:30:58	8.0	r'	-	15.7 ± 0.1	ZTF
ZTF21absvlrr	2021-08-22	08:37:29	10.0	g'	-	16.1 ± 0.1	ZTF
ZTF21absvlrr	2021-08-27	02:24:58	14.7	B	15.7 ± 0.1	15.6 ± 0.2	SUTO
ZTF21absvlrr	2021-08-27	02:30:30	14.7	V	15.6 ± 0.1	15.6 ± 0.1	SUTO
ZTF21absvlrr	2021-08-27	02:36:06	14.7	R	15.6 ± 0.1	15.6 ± 0.1	SUTO

1500, 1700000, La Serena, Chile

⁴⁷National Astronomical Research Institute of Thailand (Public Organization), 260, Moo 4, T. Donkaew, A. Mae Rim, Chiang Mai, 50180, Thailand⁴⁸OrangeWave Innovative Science, LLC, Moncks Corner, SC 29461, USA⁴⁹Department of Electronics, Electrical Engineering and Microelectronics, Silesian University of Technology, Gliwice, Poland⁵⁰Université de Strasbourg, CNRS, IPHC UMR 7178, F-67000 Strasbourg, France ⁵¹School of Physics and Astronomy, Rochester Institute of Technology, 84 Lomb Memorial Drive, Rochester, NY 14623, USA⁵²Main Astronomical Observatory of National Academy of Sciences of Ukraine, 27 Acad. Zabolotnoho Str., Kyiv, 03143, Ukraine⁵³Société Astronomique Populaire du Centre ,40 grande rue, 18340 Arçay, France

Table A2. Continued.

Source	Obs date	Time	δt (days)	filter	Detec. mag (STDpipe)	Muphoten (or ZTF)	Telescope/Observer
ZTF21absvlrr	2021-08-17	13:34:02	5.2	<i>R</i>	16.5 ± 0.1	16.5 ± 0.1	TRT-SBO
ZTF21absvlrr	2021-08-17	13:54:27	5.2	<i>I</i>	16.8 ± 0.1	16.8 ± 0.1	TRT-SBO
ZTF21absvlrr	2021-08-27	11:05:01	15.1	<i>r'</i>	-	15.5 ± 0.1	ZTF
ZTF21absvlrr	2021-08-28	02:26:24	15.7	<i>V</i>	15.7 ± 0.1	15.6 ± 0.2	SUTO
ZTF21absvlrr	2021-08-28	08:34:36	16.0	<i>g'</i>	-	15.3 ± 0.1	ZTF
ZTF21absvlrr	2021-08-28	10:03:56	16.0	<i>r'</i>	-	15.5 ± 0.1	ZTF
ZTF21absvlrr	2021-10-03	06:54:26	51.9	<i>r'</i>	-	17.7 ± 0.1	ZTF
ZTF21absvlrr	2021-10-03	08:03:41	51.9	<i>g'</i>	-	16.8 ± 0.1	ZTF
ZTF21absvlrr	2021-10-07	20:28:50	56.5	<i>V</i>	16.8 ± 0.1	17.0 ± 0.2	Terskol/Zeiss-600
ZTF21absvlrr	2021-10-07	20:29:41	56.5	<i>R</i>	16.5 ± 0.1	16.5 ± 0.2	Terskol/Zeiss-600
ZTF21absvlrr	2021-10-07	20:30:31	56.5	<i>I_c</i>	16.1 ± 0.1	16.3 ± 0.2	Terskol/Zeiss-600
ZTF21absvlrr	2021-10-08	22:12:08	57.5	<i>V</i>	17.3 ± 0.1	17.4 ± 0.2	Terskol/Zeiss-600
ZTF21absvlrr	2021-10-08	22:12:38	57.5	<i>R</i>	16.9 ± 0.1	17.1 ± 0.2	Terskol/Zeiss-600
ZTF21absvlrr	2021-10-08	22:13:09	57.5	<i>I</i>	16.5 ± 0.1	16.5 ± 0.2	Terskol/Zeiss-600
ZTF21absvlrr	2021-10-10	08:32:18	59.0	<i>g'</i>	-	17.9 ± 0.1	ZTF
ZTF21abultbr	2021-08-20	11:48:36	0.0	<i>r'</i>	-	18.8 ± 0.2	ZTF
ZTF21abultbr	2021-08-21	02:44:39	0.6	<i>R</i>	18.7 ± 0.1	18.8 ± 0.1	T-CAT
ZTF21abultbr	2021-08-21	02:44:39	0.6	<i>G</i>	18.6 ± 0.1	18.6 ± 0.1	T-CAT
ZTF21abultbr	2021-08-21	03:32:27	0.6	Clear	18.6 ± 0.2	18.2 ± 0.1	T40-A77DAU
ZTF21abultbr	2021-08-23	11:45:21	3.0	<i>r'</i>	-	18.7 ± 0.2	ZTF
ZTF21acceboj	2021-09-14	11:04:25	0.0	<i>r'</i>	-	18.4 ± 0.1	ZTF
ZTF21acceboj	2021-09-15	22:12:32	1.4	<i>g'</i>	17.9 ± 0.1	17.9 ± 0.1	BJP/ALi-50
ZTF21acceboj	2021-09-15	22:20:25	1.4	<i>r'</i>	18.0 ± 0.1	17.8 ± 0.1	BJP/ALi-50
ZTF21acceboj	2021-09-16	11:02:48	2.0	<i>r'</i>	-	17.8 ± 0.1	ZTF
ZTF21acceboj	2021-09-16	11:33:36	2.0	<i>g'</i>	-	17.8 ± 0.1	ZTF
ZTF21acceboj	2021-10-02	11:01:57	18.0	<i>r'</i>	-	17.4 ± 0.1	ZTF
ZTF21acceboj	2021-10-02	11:33:58	18.0	<i>g'</i>	-	17.8 ± 0.1	ZTF
ZTF21acceboj	2021-10-07	23:48:35	23.5	<i>V_c</i>	18.0 ± 0.1	18.3 ± 0.3	Terskol/Zeiss-600
ZTF21acceboj	2021-10-07	23:49:26	23.5	<i>R_c</i>	17.2 ± 0.2	17.2 ± 0.2	Terskol/Zeiss-600
ZTF21acceboj	2021-10-07	23:50:17	23.5	<i>I_c</i>	16.5 ± 0.1	16.6 ± 0.3	Terskol/Zeiss-600
ZTF21acceboj	2021-10-09	00:23:44	24.5	<i>V</i>	18.5 ± 0.1	18.5 ± 0.1	Terskol/Zeiss-600
ZTF21acceboj	2021-10-09	00:24:15	24.5	<i>R_c</i>	17.5 ± 0.1	17.7 ± 0.1	Terskol/Zeiss-600
ZTF21acceboj	2021-10-09	00:24:46	24.5	<i>I_c</i>	17.2 ± 0.2	17.3 ± 0.2	Terskol/Zeiss-600
ZTF21acceboj	2021-10-09	09:30:38	24.9	<i>g'</i>	-	18.0 ± 0.1	ZTF
ZTF21acceboj	2021-10-10	00:49:13	25.5	<i>V</i>	17.9 ± 0.1	18.0 ± 0.1	Terskol/Zeiss-600
ZTF21acceboj	2021-10-10	00:49:53	25.5	<i>R_c</i>	17.4 ± 0.1	17.5 ± 0.1	Terskol/Zeiss-600
ZTF21acceboj	2021-10-10	00:50:34	25.5	<i>I_c</i>	17.1 ± 0.1	16.9 ± 0.2	Terskol/Zeiss-600
ZTF21acceboj	2021-10-11	10:31:51	26.9	<i>g'</i>	-	18.0 ± 0.1	ZTF
ZTF21acceboj	2021-10-11	11:34:57	27.0	<i>r'</i>	-	17.5 ± 0.1	ZTF

⁵⁴Université Paris-Saclay, CNRS, CEA, Département d'Astrophysique, Astrophysique, Instrumentation et Modélisation de Paris-Saclay, 91191, Gif-sur-Yvette, France.

⁵⁵Astronomy and Space Physics Department, Taras Shevchenko National University of Kyiv, Glushkova ave., 4, Kyiv, 03022, Ukraine

⁵⁶National Center «Junior academy of sciences of Ukraine», 38-44, Dehtiarivska St., Kyiv, 04119, Ukraine

⁵⁷Institute of Gravitational Research, University of Glasgow, Glasgow, G12 8QQ

⁵⁸ICAAstronomy, Oria, Almería, Spain

⁵⁹Deep Sky Chile, Pichasca, Rio Hurtado, Chile

⁶⁰National University of Uzbekistan, 4 University str., Tashkent 100174, Uzbekistan

⁶¹INFN, Laboratori Nazionali del Sud, I-95125 Catania, Italy

⁶²Physics Department and Astronomy Department, Tsinghua University, <https://fr.overleaf.com/project/60fc6455b426b75b631daf74> Beijing, 100084, China